# Conformational Properties of α- or β-(1→6)-linked Oligosaccharides: Hamiltonian Replica Exchange MD Simulations and NMR Experiments

*Dhilon S. Patel[†#], Robert Pendrill[‡#], Sairam S. Mallajosyula[†], Göran Widmalm[‡*] and Alexander D. MacKerell, Jr.[†*]*

†Department of Pharmaceutical Sciences, University of Maryland, 20 Penn Street HSF II, Baltimore, Maryland 21201, USA and ‡Department of Organic Chemistry, Arrhenius Laboratory, Stockholm University, SE-106 91 Stockholm, Sweden.

* Corresponding authors. E-mails: (G.W.) gw@organ.su.se, (A.D.M.) alex@outerbanks.umaryland.edu.

# Equal contribution

**Abstract**

Conformational sampling for a set of ten α- or β-(1→6)-linked oligosaccharides has been studied using explicit solvent Hamiltonian Replica Exchange (HREX) simulations and NMR spectroscopy techniques. HREX simulations were performed to assure adequate sampling of the three dihedral angles (ϕ, ψ and ω) in the (1→6)-linkages. Validation of the force field and simulation methodology is done by comparing calculated transglycosidic *J*-coupling constants and proton-proton distances with the corresponding NMR data. Initial calculations showed poor agreement with the experimental data, prompting us to optimize the ω torsion angle parameters for (1→6)-linkages. The resulting force field is in overall good agreement with experiment, although some small limitations are evident. Detailed hydrogen bonding analysis indicates that most of the compounds lack direct intramolecular H-bonds between the two monosaccharides; however, minor sampling of the O6· · ·HO2′ hydrogen bond is present in three compounds. The results verify the role of the *gauche* effect between O5 and O6 atoms in *gluco*- and *manno*-configured pyranosides causing the ω torsion angle to sample an equilibrium between the *gt* and *gg* rotamers. Conversely, *galacto*-configured pyranosides sample a population distribution in equilibrium between *gt* and *tg* rotamers, while the *gg* rotamer populations are minor. Water radial distribution functions suggest decreased accessibility to the O6 atom in the (1→6)-linkage as compared to the O6' atom in the non-reducing sugar. The role of bridging water molecules between two sugar moieties on the distributions of ω torsion angles in oligosaccharides is also explored.

KEYWORDS: Molecular dynamics, NMR, Hamiltonian Replica Exchange, Disaccharides

## Introduction

Oligosaccharides and polysaccharides play a variety of roles in biology and biochemistry along with proteins and lipids such as storage of energy, structural roles, chemical markers, cell protectants, among others.[1-2] In biotechnology they are important in biocompatible and biodegradable materials[3-6] and carbohydrates may be a future source of renewable energy in terms of 'Biofuels'.[7-9] The diverse and complex roles of carbohydrates may be attributed to their structural diversity including a variety of functional groups, numerous stereoisomers and diversity in length, branching pattern, sequence order, and type of linkages.[10] To understand this class of molecules at a molecular level, knowledge of their three-dimensional structure and their conformational preferences in solution is essential.[11-13]

Oligosaccharides are monosaccharide units linked together via α- or β-(1→X, where, X= 1, 2,…, 6) glycosidic linkages. In addition to ring conformational preferences, the relative orientations of saccharide units are expressed in terms of the glycosidic linkage torsion angles ϕ (O5′—C1′—O6—C6) and ψ (C1′—O6—C6—C5). For (1→6)-linkages the ω torsion angle (O6—C6—C5—O5) (Scheme 1a) provides additional flexibility over other glycosidic linkages which involve only two rotatable bonds, ϕ and ψ.[14] Sampling of the ω torsion angle is described by means of the populations of the *gauche-gauche* (*gg*), *gauche-trans* (*gt*), and *trans-gauche* (*tg*) rotamers. The additional flexibility of the α- or β-(1→6)-linkages makes it more difficult to determine the preferential conformation in solution of oligosaccharides containing these linkages.[15]

Theoretical and experimental studies on the conformational preferences of the ring and rotational preferences of ω torsion angle have been carried out on monosaccharides, mainly gluco-, manno- and galactopyranosides where ω is associated with a hydroxymethyl group.[14, 16-27] In solution, ω in *gluco*- and *manno*-configured pyranosides show a preference for *gauche* (*gt* and *gg*)

orientations over the *anti*-orientation (*tg*),[16, 28-29] which is in contrast to the preference for the *tg* orientation shown in gas-phase quantum mechanics (QM) calculations.[30-32] On the other hand, ω in galactopyranosides display a high proportion of *gt* and *tg* over the *gg* rotamer in solution.[33-35] Statistical analysis of X-ray structures of glucopyranoside derivatives[36] and mannopyranoside derivatives[37] yielded a rotamer population distribution of 40:60:0 (*gt*/*gg*/*tg*) and 40:55:5 (*gt*/*gg*/*tg*), respectively. Rotamer population distributions for ω in monosaccharides are mainly attributed to the *gauche* effect,[16, 38-41] 1,3-diaxial interactions[16] and solvent effects.[42-46] In addition, NMR and Circular Dichroism (CD) data indicate that the rotamer populations of the hydroxymethyl group depend on the identity of the moiety attached at the C1 atom as well as the anomeric configuration in the reducing end residue.[47-52]

The variations in rotamer populations of ω influence the structure and function of oligosaccharides containing glycosidic (1→6)-linkages. However, the understanding of these rotamer preferences and their role in biology is still at an initial stage.[53-56] Although conformational properties of carbohydrates are difficult to establish experimentally, several NMR and molecular dynamics (MD) simulation studies have addressed the rotational and conformational preferences in these disaccharides,[57-65] as well as in larger structures.[66] In one such study, Salisburg *et al.*[67] have reported use of the Glycam force field[68] in studying conformational properties of two (1→6)-linked disaccharides (α-L-Fuc*p*-(1→6)-β-D-Glc*p*NAc-OMe and α-D-Man*p*-(1→6)-β-D-Man*p*-OMe) using an implicit water representation. In another study, the OPLS-AA-SEI force field[18, 69] was used to investigate the conformational preferences of the β-(1→6)-linkage present in β-gentiobiose using explicit solvent MD simulations and validated against data from NMR spectroscopy and X-ray crystallography.[70] Olsson *et al.*[37] reported conformational dynamics of β-D-Glc*p*NAc-(1→6)-α-D-Man*p*-OMe using a range of NMR experiments. The population

distribution around (1→6)-linkages based on MD simulations employing the PARM22/SU01[71] CHARMM-based force field was compared with experimental observation. Hünenberger and co-workers used the Gromos force field for carbohydrates[72] in combination with the local elevation umbrella sampling method to investigate conformational properties of the glucose-based (1→6)-linked disaccharides isomaltose and gentiobiose using explicit water MD simulations. Good agreement was found for ω conformational sampling in comparison to NMR spectroscopy and X-ray crystallography results.[73-74] While the above studies have yielded insights into the conformational properties of several disaccharides, concerns with respect to force field accuracy, diversity in the systems, and insufficient sampling of conformational space[23, 37, 67, 73-76] warrant further studies of these biologically interesting systems.[77]

In this study we investigate the performance of the CHARMM36 (C36) carbohydrate force field[25, 78-83] for (1→6)-linkages, especially its ability to accurately treat gluco-, manno- and galactopyranoside-based oligosaccharides. Initial results showed that the model poorly reproduces experimental data from NMR spectroscopy, motivating additional optimization of the ω dihedral parameters. New parameters for ω were subsequently optimized based on QM data on model compounds that comprise two molecules of tetrahydropyran connected by a (1→6)-linkage. To overcome issues of convergence with respect to the sampling of conformational space, we employ Hamiltonian Replica Exchange (HREX) based simulations. The force field is validated by comparing transglycosidic *J* coupling constants and proton-proton distances from the simulations with NMR observations. Detailed molecular level analysis is performed to characterize the role of water in the conformational flexibility of the (1→6)-linked oligosaccharides.

## Methods

### *NMR Spectroscopy*

Oligosaccharides **1** – **10** (~10 mg), available from previous studies,[37, 61, 84-87] were lyophilized from $D_2O$ prior to dissolution in 0.6 mL $D_2O$. NMR experiments were performed at 298 K on a Bruker Avance III 700 MHz spectrometer equipped with a 5 mm TCI Z-gradient Cryoprobe, unless otherwise stated. Gradient pulses were of 1 ms length unless otherwise stated.

Homonuclear proton-proton coupling constants for all compounds and heteronuclear carbon-proton coupling constants for the site-specifically labeled compounds, viz. [6-$^{13}$C]-**3** and [1',6-$^{13}C_2$]-**3**, were obtained through iterative fitting of spin-simulated spectra to experimental 1D $^1$H spectra using the PERCH NMR spin simulation software.[88]

Heteronuclear $J_{CH}$ were determined using the constant time J-HMBC experiment reported by Meissner and Sørensen,[89] with a low-pass *J* filter with $\tau_1$ = 3.45, $\tau_2$ = 3.13 and $\tau_3$ = 2.78 ms being used to suppress one-bond $^{13}$C,$^1$H correlations. For $^{13}$C nuclei, inversion during the coupling evolution was achieved using an 80 kHz Chirp pulse (0.5 ms, 20% smoothing) whereas for refocusing during chemical shift evolution an 80 kHz composite Chirp pulse (2 ms, 20% smoothing) was used. Typically, three to four experiments were acquired for each compound with different coupling evolution delays (Δ) in the range 0.56 – 0.83 s. For compound **6**, an additional experiment was performed with Δ set to 0.29 s, whereas for compound **5**, five experiments with Δ in the range 0.42 – 0.71 s were used. Three experiments for compound **10** were used in which Δ was set to 0.42, 0.56 and 0.63 s. Spectral widths were 2.5 – 5.0 ppm and 60 – 80 ppm in the direct and indirect dimensions, respectively. The acquisition times were 0.6 – 2 s and delay of 1 – 1.4 s was used between transients. In the indirect dimension, 128 – 512 $t_1$ increments were used, averaging 4 – 32 transients per increment. For all cases, the maximum possible scaling factor (κ) was used, i.e. $\kappa = \Delta/t_{1,max}$. Linear prediction to 256 – 1024 points, zero-filling to 4096 points and multiplication by a squared 90° shifted sine-bell function were performed prior to Fourier

transformation along the indirect dimension. Coupling constants were determined from the scaled peak separation in magnitude mode projections of the indirect dimension.

The HSQC-HECADE[90] experiment was used for the measurement of $^{2}J$(H5,C6) heteronuclear coupling constants in compounds **4**, **5**, **6**, **9** and **10** and for $^{3}J$(C4,H6*R*) in **5**. The $^{1}J_{CH}$ scaling factor was set to 0.4 for compounds **4**, **5**, **6** and **9** and to 0.3 for compound **10**, and the isotropic mixing time was 60 ms. For compounds **4**, **5**, **6** and **9** the spectral width was 3 ppm and 60 ppm in the direct and indirect dimension, respectively, and 2 transients were averaged for each of the 512 increments. The acquisition time in the direct dimension was 2 s. For compound **10**, the number of increments was 1024 and the spectral widths were 5 ppm and 70 ppm in the direct and indirect dimensions, respectively; for each increment, 4 transients were averaged using an acquisition time of 3 s. The direct dimension was zero-filled to a digital resolution of 0.1 Hz per point and multiplied with a 2 Hz exponential line-broadening function, while the indirect dimension was subjected to linear prediction and zero-filling to 8192 data points, and multiplied by a squared 90° shifted sine-bell function prior to Fourier transformation. Coupling constants were determined by comparing 1D projections for the different spin states.

$^{1}$H,$^{1}$H cross-relaxation rates in compounds **6** and **8** were determined on a Bruker Avance III 600 MHz spectrometer equipped with a 5 mm TXI Z-gradient probe using a 1D SPFGSE NOESY experiment.[91] Zero-quantum coherences were dephased[92] at the end of the mixing time by the simultaneous application of a 2 G·cm$^{-1}$ gradient pulse and a 20 kHz Chirp pulse (10 ms, 20% smoothing). The 180° pulse at the center of the mixing time was flanked by 22 G·cm$^{-1}$ gradient pulses of opposite directions. Selective excitation was achieved by a r-SNOB shaped pulse[93] flanked by gradient pulses with the strength 8 G·cm$^{-1}$. The length of the selective pulse was 80 ms for H1' in **6** and **8**, 100 ms for H4 in **6** and 150 ms for H5 in **8**. For each excitation, 6

mixing times between 50 and 500 ms were used and each experiment was performed three times in a random order. The spectral window of 10 ppm was sampled with 32k points and the repetition time was 15 s. Prior to Fourier transformation, the FIDs were zero-filled to 256k points and multiplied by 0.3 Hz exponential line-broadening functions. Baseline correction and integration was performed using the same regions for all spectra having the same excitation. The integrals of relevant peaks were divided by that of the excited resonance,[94] before fitting of second order equations in which the linear terms correspond to the cross-relaxation rates (σ). Quadratic terms were excluded if an *F*-test yielded Pr(>*F*) = 0.01 or higher. For the excitation of H1' in compound **6**, the integrated region for H6*S* overlapped with that of H3', H5' and H6'*R*, and the region for H6*R* overlapped with H5 and H6'*S*. The estimated contributions from the intra-residue interactions were subtracted from the observed cross-relaxation rates, using the effective distances from the MD simulation.[95] Effective distances were calculated using the isolated spin-pair approximation. The value of $\sigma_{\mathrm{ref}} \cdot r_{\mathrm{ref}}^6$ was calculated for all available reference interactions using effective distances from the MD simulations and the average of these, $\langle \sigma_{\mathrm{ref}} \cdot r_{\mathrm{ref}}^6 \rangle$, was then used to calculate $r_{ij}$ according to $r_{ij}^6 = \langle \sigma_{\mathrm{ref}} \cdot r_{\mathrm{ref}}^6 \rangle / \sigma_{ij}$ for the interaction between protons *i* and *j*. For compound **6**, the interactions of H1' with H2' and H4', and of H4 with H1, H2 and H3 were used, giving $\langle \sigma_{\mathrm{ref}} \cdot r_{\mathrm{ref}}^6 \rangle$ = 11.6 $\text{Å}^6 \cdot \text{s}^{-1}$, and for compound **8**, the interactions of H1' with H2', H3', H4' and H5', and the H5–H1 interaction were used, giving $\langle \sigma_{\mathrm{ref}} \cdot r_{\mathrm{ref}}^6 \rangle$ = 14.4 $\text{Å}^6 \cdot \text{s}^{-1}$. From the T-ROESY cross-relaxation rates reported by Lycknert *et al.*[84] for compound **2**, the value $\langle \sigma_{\mathrm{ref}} \cdot r_{\mathrm{ref}}^6 \rangle$ = 23.5 $\text{Å}^6 \cdot \text{s}^{-1}$ was determined.

***Computational Details***

QM calculations were performed with the Gaussian03 software[96] using the MP2/cc-pVTZ//MP2/6-31G* model chemistry. Optimizations were performed to default tolerances.

Empirical force field calculations were performed using the program CHARMM[97] with the CHARMM36 carbohydrate force field[78] and the CHARMM modified TIP3P water model.[98] Initial conformations of the model compounds were generated from the topology information present in the force field and were subjected to a 1000-step steepest descent (SD) energy minimization followed by an Adopted Basis Newton Raphson (ABNR) energy minimization to a force gradient tolerance of $10^{-6}$ kcal·mol$^{-1}$·Å$^{-2}$.[99-100] The energy minimized oligosaccharides were then immersed in a pre-equilibrated cubic water box of size 32 Å × 32 Å × 32 Å, which extends at least 10 Å beyond the non-hydrogen atoms of the oligosaccharides. Over-lapping water molecules within 2.8 Å of non-hydrogen solute atoms were deleted. For all of the subsequent minimizations and MD simulations, periodic boundary conditions were employed using the CRYSTAL module implemented in the CHARMM program. The electrostatic interactions were treated via the particle-mesh Ewald method[101] with a real-space cutoff of 12 Å and non-bonded interaction lists were updated heuristically out to 16 Å with a force switch smoothing function from 10 to 12 Å used for the Lennard-Jones interactions.[102] The system was heated during 100 ps from 100 K to 298 K with 2.0 kcal·mol$^{-1}$·Å$^{-2}$ harmonic restraints on the non-hydrogen atoms of the solutes. This was followed by equilibration during 200 ps using the NVT ensemble with 1.0 kcal·mol$^{-1}$·Å$^{-2}$ harmonic restraints on the non-hydrogen atoms of the oligosaccharides. Subsequently, a 200 ps NPT simulation at 1 atm and 298 K was performed without restraints except for the SHAKE algorithm, which was used to constrain hydrogen atoms involved in covalent bonds.[103] The center of mass (COM) of the solutes was restrained near the origin by using the MMFP module[104] in CHARMM using a harmonic restraint of 1.0 kcal·mol$^{-1}$·Å$^{-2}$.

The REPDSTR module of a modified version of CHARMM c37b2 was used to perform the HREX simulations.[105] The HREX simulations were started from the equilibrated coordinates

and were carried out for 11 ns for each replica in the NPT ensemble using the system setup described above including the COM harmonic restraint. An exchange between neighboring replicas was attempted every 1000 MD steps, and the coordinates were saved every 1 ps. For all analyses, the trajectories obtained from the last 10 ns of the unperturbed replica (unbiased, ground state replica out of 8 replicas) were used.

Different HREX strategies and its application to biological systems have been reported in the literature.[106-111] In the present study, a combination of the two-dimensional (2D) dihedral grid-based energy correction map (CMAP)[112] and a Saxon-Wood potential[113] as the biasing potential across the different replicas, is used. CMAP biasing potentials (bpCMAP) are used corresponding to the ψ/ω dihedrals while a Saxon-Wood potential is used to enhance conformational sampling about the ϕ dihedral angle. To arrive at the bpCMAPs the underlying MM 2D free energy profiles were obtained by the following procedure. The conformational distribution of each disaccharide in vacuum was sampled using high temperature gas phase Langevin dynamics simulations at 500 K for 500 ns. 2D dihedral distributions for ψ/ω were computed from snapshots saved every 2 ps from the simulations. These 2D dihedral distributions were then converted to free energy profiles based on a Boltzmann probability distribution. The free energy surfaces were then used to generate the eight CMAPs for the eight replicas by scaling the free energy surface by a factor –0.15*n*, where *n* was varied from 0 to 7. Thus, the first replica with 0% scaling represents a simulation with no perturbing potential and the subsequent replicas are under an influence of 15, 30, 45, 60, 75, 90 and 105% of the respective bpCMAPs. An example of a ψ/ω bpCMAP is presented in Figure S1 of the supporting information. For the ϕ dihedral the Saxon-Wood potential utilized a scaled force constant term as the biasing potential across the replicas (Eq. 1).

$$\boldsymbol{U = h[1 + exp\left\{\frac{P2 - |\,\theta - \theta ref\,|}{P1}\right\}]^{-1}} \quad \text{------ (1)}$$

where $h = -0.15n$ kcal·mol$^{-1}$ , with $n$ going from 0 to 7 for replicas 1–8; $P_1 = 0.1$; $P_2 = 0.3$; and $\theta_{ref} = 60°$ (**1**, **4**, **6**, **8** and **10**) and –75° (**2**, **3**, **5**, **7** and **9**). $\theta_{ref}$ was set to the local minimum from a dihedral scan about ϕ in each system.

***Calculation of J Coupling Constants***

Sampling of the three conformational states of ω, i.e. *gt* (staggered conformation at 60°), *gg* (–60°) and *tg* (180°) can be determined from the homonuclear $^3J$(H5,H6*R*) and $^3J$(H5,H6*S*) coupling constants.[16, 21] Different Karplus equations for these coupling constants have been proposed by Haasnoot *et al*.,[114] Imay and Osawa[115] and Stenutz *et al*.[116] The modified Karplus equations proposed by Stenutz *et al*. for $^3J$(H5,H6*R*) and $^3J$(H5,H6*S*), equations 2 and 3, respectively, were derived from combined experimental and computational density functional theory (DFT) studies.[116] Continuing these efforts, Thibaudeau *et al*. proposed that the conformational distribution of the ω torsion angle can also be correlated with the $^2J$(H5,C6) and $^2J$(C4,C6) coupling constants as given in eq. 4 and 5.[117]

$^3J$(H5,H6*R*) = 5.08 + 0.47cos (ω) + 0.90sin (ω) – 0.12cos (2ω) + 4.86sin (2ω) ….(2)

$^3J$(H5,H6*S*) = 4.92 – 1.29cos (ω) + 0.05sin (ω) + 4.58cos (2ω) + 0.07sin (2ω) ….(3)

$^2J$(H5,C6) = –1.29 + 1.53cos (ω) – 3.68sin (ω) ……(4)

$^2J$(C4,C6) = 0.02 + 0.16cos (ω) + 1.34sin (ω) …….(5)

In this work, we used eq. 2 and 3 to calculate $^3J$(H5,H6*R*) and $^3J$(H5,H6*S*) coupling constants for the C5–C6 torsion angle in the reducing end residue as well as in the terminal residue.

Heteronuclear proton-carbon coupling constants, $^3J$(C6,H1′), which are related to ϕ (O5′—C1′—O6—C6) were analyzed using a Karplus equation developed by Widmalm *et al.* as shown in eq. 6.[118]

$^3J$ (C6,H1′) = 6.54cos$^2$ ($\phi_H$ - Δ) – 0.62cos ($\phi_H$ - Δ) – 0.17 …….(6)

where $\phi_H$ = H1′—C1′—O6—C6. The phase shift, Δ, which is dependent on the stereochemistry of the linkage between the sugar residues, is –12° for α-D-hexopyranosides and β-L-hexopyranosides and +12° for β-D-hexopyranosides and α-L-hexopyranosides.

Heteronuclear proton-carbon coupling constants, $^3J$(C1′,H6*R*/*S*), were calculated from the simulations using eq. 7.[118]

$^3J$(C1′,H6*R*/*S*) = 6.54cos$^2$ ($\psi_H$) – 0.62cos ($\psi_H$) + 0.33 + 0.6 exp (κcos ($\phi_{O5'}$ – 180))/exp(κ) …….(7)

where $\psi_{HR/S}$ = C1′-O6-C6-H6*R*/*S*. The variable in-plane effect factor, *κ*, is 8 and $\phi_{O5'}$ is the torsion angle involving the O5′ oxygen atom of the terminal residue.

Coupling constants were calculated every 1 ps from the unperturbed replicas, amounting to 10000 points (10 ns) from the HREX MD simulations.

**Results and Discussion**

The conformational preferences of the α- or β-(1→6)-linkaged oligosaccharides, in terms of three dihedral angles, ϕ, ψ and ω, were investigated using conformationally sensitive experimental parameters from NMR spectroscopy, as well as HREX aqueous MD simulations, using the herein optimized force field parameters, for disaccharides **1** – **9** and trisaccharide **10** (Scheme 1). Moreover, conformational preferences at ω′ (O6′—C6′—C5′—O5′) were analyzed for disaccharides **1 – 7**. The compounds include gluco-, manno- and galactopyranosides as *O*-methyl

glycosides of the reducing end residue and gluco-, manno-, galacto- and fuco-pyranosides at the non-reducing end, with α- or β-configurations at the anomeric carbons. Because of differences in stereo-electronic properties, differences in rotamer populations around ω are expected.[15-16]

***NMR Spectroscopic Data for Glycosidic (1→6)-Linkages***

Homonuclear $^{1}$H,$^{1}$H coupling constants were determined for all compounds by total line-shape analysis[88] of experimentally determined 1D $^{1}$H spectra. This gave values, shown in Table 1, for $^{3}J$(H5,H6*R*) and $^{3}J$(H5,H6*S*) which report on the conformational preferences at the ω torsion angle, as well as $^{2}J$(H6*R*,H6*S*) coupling constants (Table S1 in the Supporting Information), which are sensitive to both the ω and ψ torsion angles. Compound **3** was available also as the [6-$^{13}$C] and [1',6-$^{13}C_2$] site-specifically labeled isotopologues and thus it was possible to determine the values for the $^{3}J$(H1',C6), $^{3}J$(C1',H6*R*) and $^{3}J$(C1',H6*S*) coupling constants using the total line-shape analysis approach as demonstrated in Figure 1. For samples at natural $^{13}$C abundance, the J-HMBC and HSQC-HECADE experiments were used for the determination of heteronuclear $^{13}$C,$^{1}$H long-range coupling constants, as shown for compound **5** in Figure 2. The resulting values are shown in Tables 2 and 3.

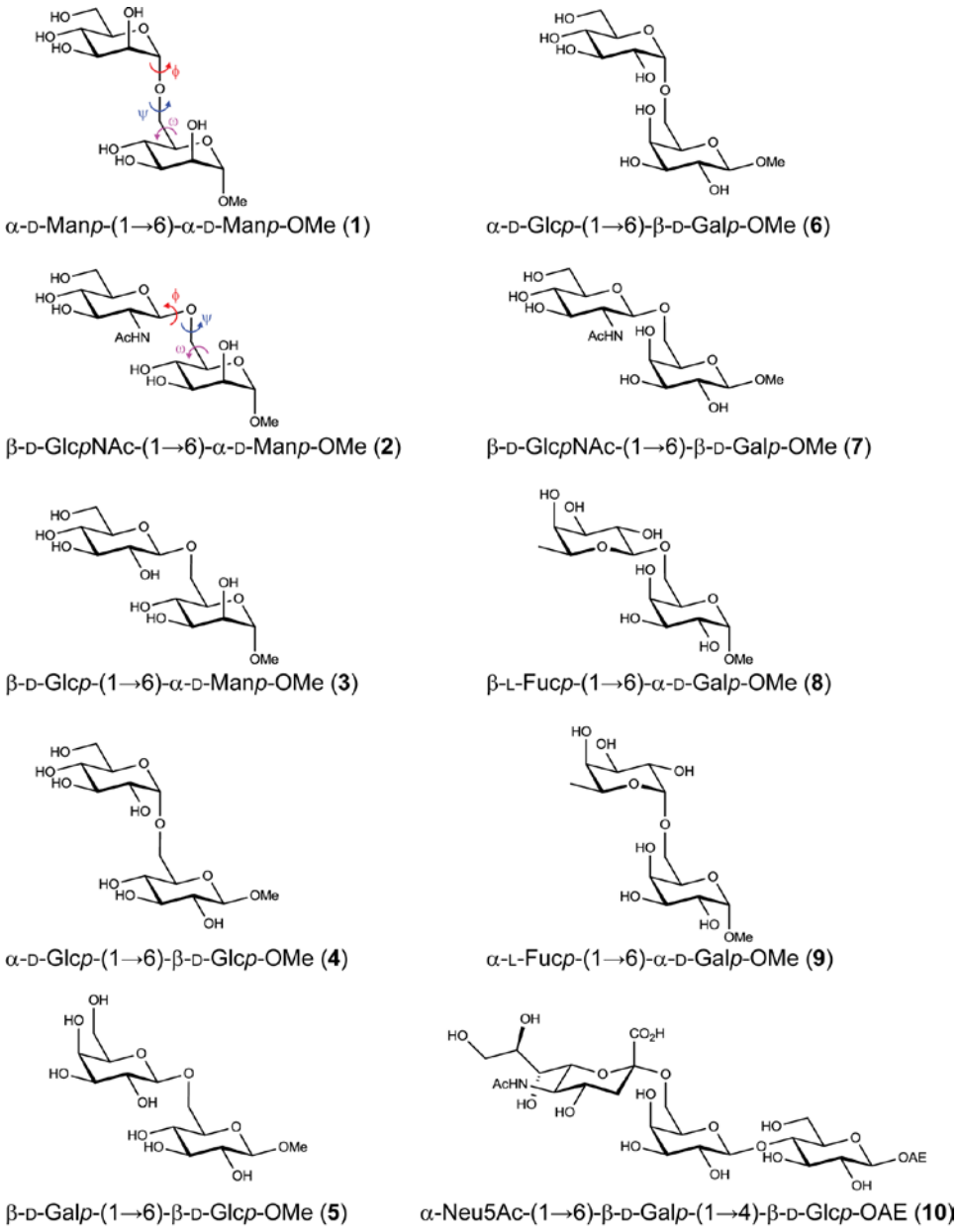


**Scheme 1.** Schematic representation of the *manno*- (**1 – 3**) *gluco*- (**4 – 5**) and *galacto*- (**6 – 10**) configured (1/2→6)-linked pyranosides included in the current study.

Using limiting values for $^{3}J$(H5,H6*R*) and $^{3}J$(H5,H6*S*),[116] the relative populations of the three staggered rotamers *gt*, *gg* and *tg* at the ω and ω' torsion angles were determined (Table 4). The resulting populations are in agreement with previous studies in that for manno- and glucopyranosides, there is an approximately equal population of the *gt* and *gg* rotamers and limited

populations of *tg*, whereas for galactopyranosides the populations are *gt* > *tg* ≫ *gg*.[117] Generally, the population of the *gt* rotamer at the ω torsion angle was found to be higher in the β-D/α-L-linked compounds than in the α-D/β-L-linked compounds, in agreement with findings in a previous study of (1→6)-linked disaccharides.[61] Thus, the population of *gt* is larger in the β-D-linked compounds **2**, **3** and **5** than in the α-D-linked compounds **1** and **4**. Similarly, the population of *gt* is larger in compounds **7** (β-D) and **9** (α-L) than in compounds **6** (α-D) and **8** (β-L).

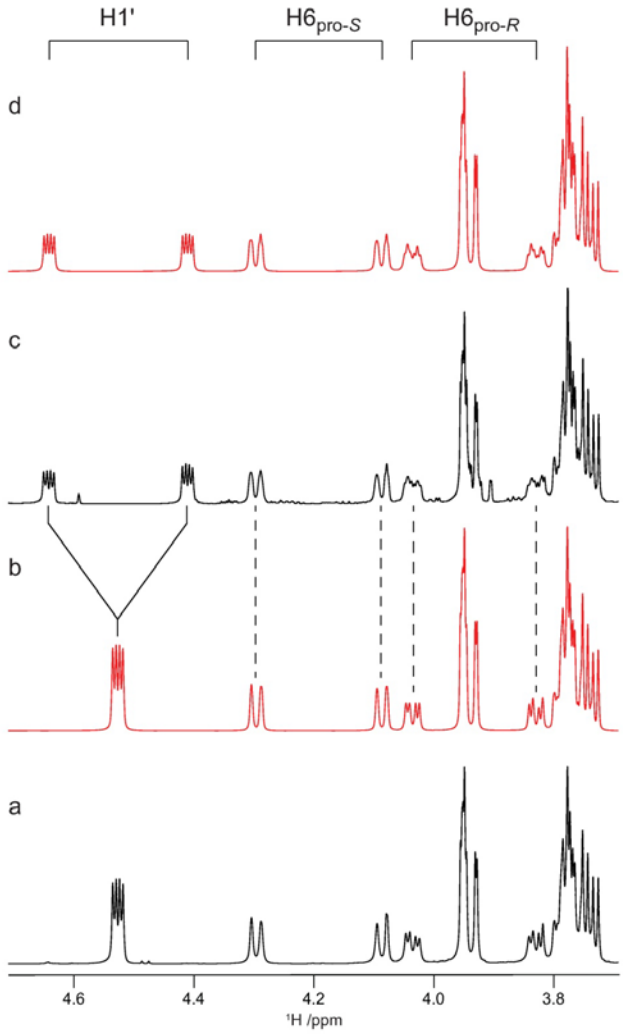


**Figure 1.** Selected region of1D $^{1}H$ spectra for the site-specifically $^{13}C$ labeled isotopologues of compound **3**. Experimental (a) and spin-simulated (b) spectra for [6-$^{13}C$]-**3** and experimental (c) and spin-simulated (d) spectra for [1',6-$^{13}C_2$]-**3**.

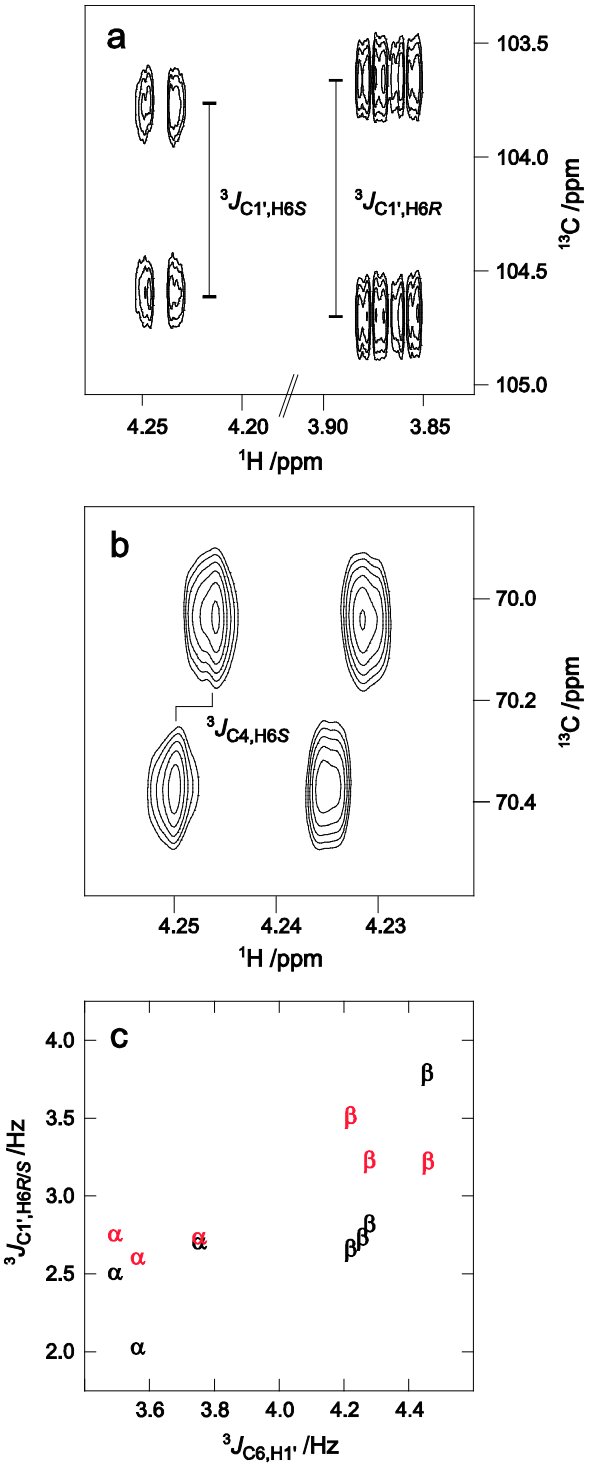


**Figure 2.** Examples of NMR spectra used in the determination of heteronuclear long-range coupling constants in compound **5**; (a) determination of $^3J$(C1',H6*R*) and $^3J$(C1',H6*S*) using the J-HMBC experiment, (b) determination of $^3J$(C4,H6*S*) using the HSQC-HECADE experiment. (c) Correlation between the values for $^3J$(C1',H6*R*) (red), $^3J$(C1',H6*S*) (black), and $^3J$(C6,H1') in compounds **1 – 8** labeled according to the stereochemistry at the anomeric carbon of the terminal residue.

**Table 1.** $^{2}J$ and $^{3}J$ coupling constants (in Hz) for **1** – **9** associated with ω (O5—C5—C6—O6) and ω′ (O5′—C5′—C6′—O6′) obtained from experiments and calculated based on dihedral distributions from HREX MD simulations (10 ns).

| Compound | ω (O5—C5—C6—O6) | | | | | | | | ω′ (O5′—C5′—C6′—O6′) | | | |
|---|---|---|---|---|---|---|---|---|---|---|---|---|
| | $^{3}J$(H5,H6*R*) | | $^{3}J$(H5,H6*S*) | | $^{2}J$(H5,C6) | | $^{2}J$(C4,C6) | | $^{3}J$(H5,H6*R*) | | $^{3}J$(H5,H6*S*) | |
| | Expt. | Calc. | Expt. | Calc. | Expt. | Calc. | Expt. | Calc. | Expt. | Calc. | Expt. | Calc. |
| **1**[a] | 5.12 | 5.12 | 1.96 | 1.81 | –1.69[b] | –0.19 | <0.5 | 0.12 | 5.98 | 6.69 | 2.20 | 2.27 |
| **2**[a] | 6.48 | 6.10 | 1.91 | 1.79 | –2.15[b] | –1.11 | <0.5 | 0.44 | 5.77 | 5.06 | 2.19 | 2.10 |
| **3** | 5.41 | 5.36 | 2.03 | 1.76 | –1.29[b] | –0.44 | <0.5 | 0.21 | 6.13 | 6.37 | 2.31 | 2.32 |
| **4** | 4.32 | 4.15 | 2.13 | 1.79 | –1.0 | –0.22 | -[c] | 0.12 | 5.15 | 5.87 | 2.30 | 2.18 |
| **5** | 5.64 | 6.11 | 2.07 | 1.84 | –1.7 | –1.02 | - | 0.42 | 7.93 | 6.77 | 4.35 | 5.34 |
| **6** | 7.19 | 7.02 | 5.08 | 4.04 | –5.8 | –2.64 | - | 0.74 | 5.33 | 6.85 | 2.29 | 2.31 |
| **7** | 7.78 | 7.74 | 4.13 | 3.47 | - | –3.09 | - | 0.96 | 5.82 | 5.56 | 2.20 | 2.27 |
| **8** | 7.35 | 6.32 | 4.97 | 4.45 | - | –2.32 | - | 0.59 | | | | |
| **9** | 7.74 | 7.67 | 4.61 | 4.52 | –5.4 | –3.28 | - | 0.92 | | | | |

Expt. – Experimental, Calc. – Calculated
[a]Experimental values from reference 37.
[b]Obtained by total line-shape analysis of site-specifically labeled $^{13}$C isotopologues.
[c]Not determined.

**Table 2.** $^{3}J$ coupling constants (in Hz) of **1** – **9** associated with ϕ (O5′—C1′—O6—C6) obtained from experiments and calculated based on dihedral distributions from HREX MD simulations (10 ns).

| | $^{3}J$(C6,H1′) | |
|---|---|---|
| **Compound** | **Expt.** | **Calc.** |
| **1** | 3.36 | 3.16 |
| **2** | 4.10[a] | 3.34 |
| **3** | 4.26[b] | 3.42 |
| **4** | 3.56 | 3.30 |
| **5** | 4.22 | 3.39 |
| **6** | 3.75 | 3.31 |
| **7** | 4.35 | 3.34 |
| **8** | 4.46 | 3.31 |
| **9** | -[c] | 3.28 |

Expt. – Experimental, Calc. – Calculated
[a]Experimental value from reference 37.
[b]From total line-shape analysis of [6-$^{13}$C]-**3** and [1',6-$^{13}C_2$]-**3**, the value was 3.89 and 3.91 Hz, respectively.
[c]Not determined.

**Table 3.** $^{3}J$ coupling constants (in Hz) of **1 – 9** associated with ψ (C1′—O6—C6—C5) obtained from experiments and calculated based on dihedral distributions from HREX MD simulations (10 ns).

| | $^{3}J$ (C1′,H6*R*) | | $^{3}J$ (C1′,H6*S*) | |
|---|---|---|---|---|
| **Compound** | **Expt.** | **Calc.** | **Expt.** | **Calc.** |
| **1** | 2.75 | 2.74 | 2.50 | 2.08 |
| **2** | -[a] | 2.74 | - | 1.85 |
| **3** | 3.23[b] | 2.13 | 2.82[b] | 2.19 |
| **4** | 2.60 | 2.51 | 2.02 | 1.74 |
| **5** | 3.51 | 2.47 | 2.66 | 2.04 |
| **6** | 2.73 | 2.61 | 2.70 | 1.93 |
| **7** | - | 2.34 | 2.73 | 2.25 |
| **8** | 3.22 | 2.61 | 3.79 | 2.37 |
| **9** | 2.80 | 1.85 | 3.20 | 2.52 |

Expt. – Experimental, Calc. – Calculated
[a]Not determined
[b]From total line-shape analysis of [1',6-$^{13}C_2$]-**3**, the values were 3.1 and 2.7 Hz for H6*R* and H6*S*, respectively.

The coupling constant, $^{3}J$(H1',C6), related to the ϕ torsion angle, was found to be around 4.3 Hz in the β-linked compounds and around 3.7 Hz in the α-linked compounds (Table 2, Figure 2c), indicating a slight difference in the conformational preferences depending on the anomeric configuration. Both of the $^{3}J$(C1',H6*R*) and $^{3}J$(C1',H6*S*) coupling constants (Table 3), related to the ψ torsion angle, were slightly larger in the β-linked compounds. For all disaccharides with α-D or β-D configuration at the terminal end residue (**1** – **7**), $^{3}J$(C1',H6*R*) > $^{3}J$(C1',H6*S*) where experimental data is available, whereas for the two compounds with L-configuration at this residue (**8** and **9**), the reverse order was observed.

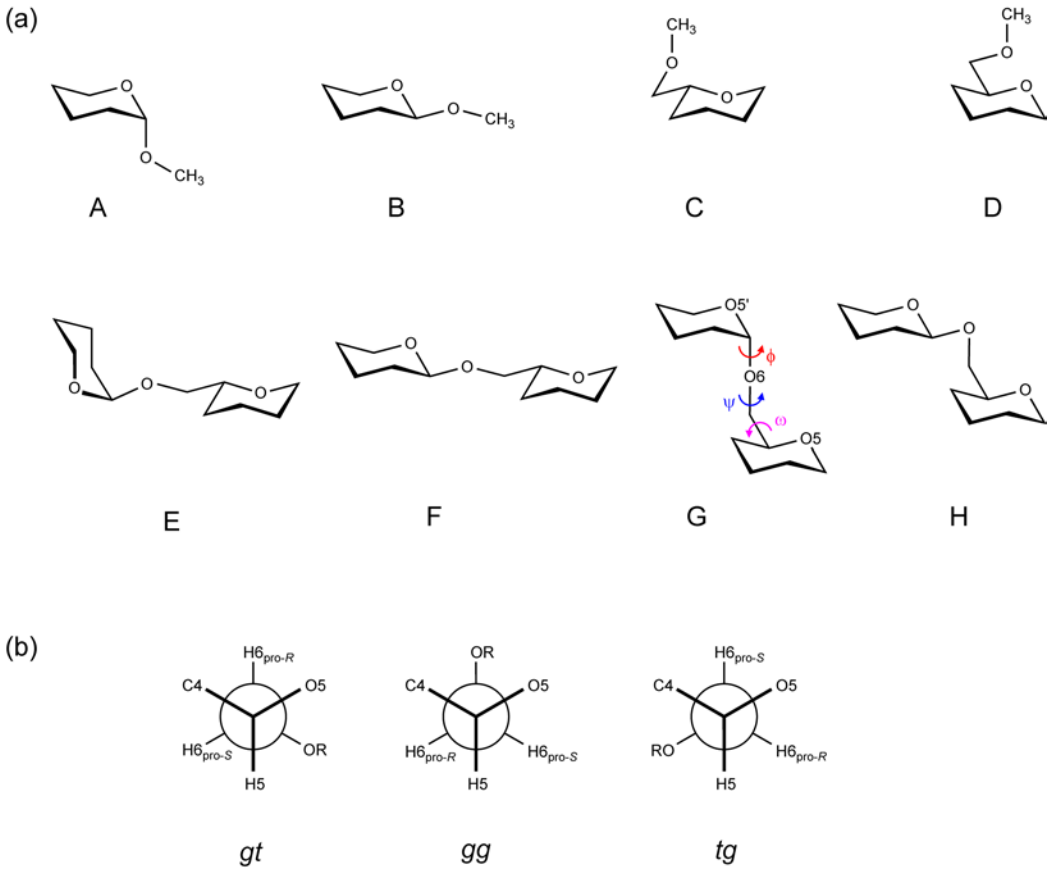


**Scheme 2.** (a) Schematic representation of model compounds. **A** – **D** are model compounds used previously and **E** – **H** represent the new model compounds used for deriving dihedral parameters for the ω torsion angle. (b) Newman projection of ideal staggered ω rotamers about the C5—C6 bond.

***Parametrization and Computational Data of Glycosidic (1→6)-Linkages***

The reported parameters for the glycosidic (1→6)-linkage in the CHARMM36 carbohydrate force field, which are represented by ϕ = $O'_{ring}$—C1′—$O_{link}$—C6, ψ = C1′—$O_{link}$—C6—C5 and ω = $O_{link}$—C6—C5—$O_{ring}$ torsion angles, were developed based on model compounds **A** and **B** for ϕ and **C** and **D** for ψ and ω (Scheme 2), in part due to the computational cost associated with the QM calculations needed to generate target data.[78] Optimization using **A** – **D** gave ψ/ω surfaces and $O_{link}$—C6—C5 angle geometries in good agreement with QM data. However, analysis of the population distribution around ω was not studied using explicit solvent MD simulations. This was

undertaken in the present study, where our preliminary calculations using both standard MD and HREX simulations were unable to reproduce the correct ω conformational preferences for the molecules included in this study (Table S2 and S3, supporting information). This motivated additional optimization of the ω torsion parameters.

To re-parameterize the ω torsion angle, QM calculations were performed on model compounds that consist of two tetrahydropyran units connected by (1→6)-linkages. All of the four possible configurations at both of the C1′ and C5 sites were considered (**E** – **H**, Scheme 2). Full QM scans for all three torsion angles (ϕ, ψ and ω) with the new model compounds would be computationally expensive, thus a knowledge-based set of 192 conformations were optimized by constraining ϕ (O5′—C1′—O6—C6) to 60° or –60° and ψ (C1′—O6—C6—C5) to 180° while scanning ω (O6—C6—C5—O5) from –180° to 165° at an interval of 15°. During the optimization we explored the possibility of both phase variation (i.e. phases allowed to assume any value) and non-phase variation (i.e. phase = $0^0$ or 180˚) with multiplicities of 1, 2 and 3. The results discussed below are based on parameters obtained through the non-phase variation method, consistent with other dihedral parameters in the carbohydrate force field. Potential energy plots with parameters developed based on phase variation and non-phase variation during dihedral fitting are given in the Figure S2 and S3, respectively, in the supporting information. The optimization lead to satisfactory agreement with the QM data, while the enforcement of the phase to 0° or 180° required empirical adjustment of the dihedral parameter for the O6—C6—C5—C4 torsion angle. A somewhat decreased ability of the model to reproduce the QM data was required to balance the rotamer equilibrium between *gt* and *gg* in gluco- and mannopyranosides and between *gt* and *tg* in galactopyranosides. For example, the root mean square (RMS) energy difference over 192 conformations was 0.68 kcal·mol$^{-1}$ for the original C36 parameters, 1.01 kcal·mol$^{-1}$ for the phase

restrained optimized parameters and 1.02 kcal·mol$^{-1}$ for the parameters from phase variation. For illustrative purposes, ω sampling for compounds **1** and **2** from the HREX simulations using the original C36 and the new parameters are given in supporting information Figure S4. The original C36 parameters, despite being in better agreement with the gas phase QM data, were found to be biased towards *gg* conformational sampling in all compounds.

***Conformational Analysis of ω Torsion Angles (O5—C5—C6—O6)***

The results of four different types of *J* couplings that are dependent on ω, viz. $^{3}J$(H5,H6*R*), $^{3}J$(H5,H6*S*), $^{2}J$(H5,C6) and $^{2}J$(C4,C6) calculated from the HREX simulations are presented in Table 1. In general, calculated $^{3}J$(H5,H6*R*) coupling constants are larger than $^{3}J$(H5,H6*S*) and agree very well with experimental observations. Disaccharides **1 – 5**, having *manno*- or *gluco*-configuration at the reducing end residue, show lower values for both of the $^{3}J$(H5,H6*R*) and $^{3}J$(H5,H6*S*) coupling constants than disaccharides **6 – 9** with *galacto*-configuration in this residue, in the experimental measurements as well as from the simulations. The calculated $^{3}J$(H5,H6*R*) and $^{3}J$(H5,H6*S*) values generally agree within ~ 0.5 Hz, although slightly larger deviations from the experimental values were observed in compounds **6 – 8**.

**Table 4.** ω and ω′ rotamer distributions of the compounds **1 - 9** using HREX MD (10 ns). Distributions are binned from 0° to 120° for *gt*, from –120° to 0° for *gg*, and from 120° to 180° and –120° to –180° for *tg* rotamers in the interval –180° to 180°.

| **Compound** | **ω (O5—C5—C6—O6) Population (%)** | | | | | | **ω′ (O5'—C5'—C6'—O6') Population (%)** | | | | | |
|---|---|---|---|---|---|---|---|---|---|---|---|---|
| | ***gt*** | | ***gg*** | | ***tg*** | | ***gt*** | | ***gg*** | | ***tg*** | |
| | **Expt.** | **Calc.** | **Expt.** | **Calc.** | **Expt.** | **Calc.** | **Expt.** | **Calc.** | **Expt.** | **Calc.** | **Expt.** | **Calc.** |
| **1** | 45 | 44.6 | 49 | 54.4 | 6 | 1.0 | 54 | 63.3 | 38 | 31.2 | 8 | 5.5 |

| | | | | | | | | | | | | |
|---|---|---|---|---|---|---|---|---|---|---|---|---|
| **2** | 60 | 57.0 | 35 | 41.9 | 5 | 1.1 | 51 | 45.6 | 41 | 50.0 | 8 | 4.4 |
| **3** | 48 | 48.1 | 46 | 51.7 | 6 | 0.2 | 55 | 60.5 | 36 | 33.0 | 9 | 6.5 |
| **4** | 35 | 35.3 | 57 | 64.5 | 8 | 0.3 | 44 | 54.6 | 47 | 40.3 | 9 | 5.1 |
| **5** | 50 | 56.8 | 43 | 42.8 | 7 | 0.4 | 66 | 55.1 | 3 | 1.9 | 31 | 43.0 |
| **6** | 55 | 59.3 | 7 | 15.0 | 38 | 25.7 | 46 | 61.7 | 45 | 32.0 | 9 | 6.3 |
| **7** | 65 | 70.5 | 7 | 9.6 | 28 | 19.9 | 52 | 51.0 | 40 | 42.6 | 8 | 6.4 |
| **8** | 57 | 50.5 | 6 | 19.6 | 37 | 29.9 | | | | | | |
| **9** | 63 | 64.7 | 4 | 4.7 | 33 | 30.6 | | | | | | |

Expt. – Experimental, Calc. – Calculated

The population distribution of ω (Table 4) shows that for **1 – 5** the *gt* and *gg* rotamers were significantly populated while the population of the *tg* rotamer was negligible. This is due to stabilization of the *gg* and *gt* rotamers in gluco- and mannopyranosides by the *gauche* effect between O5 and O6 as well as destabilization of the *tg* rotamer due to the 1,3-diaxial interaction between O4 and O6.[28] For **6 – 9**, ω populates the *gt* and *tg* rotamers whereas population of the *gg* rotamer is suppressed due to the 1,3-diaxial interaction between O4 and O6.[28] The larger values of the $^{3}J$(H5,H6*R*) and $^{3}J$(H5,H6*S*) coupling constants in **6 – 9** as compared with **1 – 5** are attributed to lower populations of the *gg* rotamers and higher populations of the *tg* rotamers in the former compounds. The minor discrepancies between calculated and experimental $^{3}J$ values could be traced back to rotamer populations in **1 – 9**. For instance, the larger deviation of the *gt* rotamer population found in **5** is clearly reflected in the discrepancy between calculated and experimental values for $^{3}J$(H5,H6*R*) for compound **5**. In addition, the simulations slightly overestimate the *gg* populations and underestimate the *tg* populations for **6 – 8**, resulting in underestimated values for the $^{3}J$(H5,H6*S*) coupling constants. However, excellent agreement between calculated and experimental rotamer distribution was obtained for **9**.

The calculated $^{2}J$(C4,C6) coupling constants with values of ~ 0.5 Hz and negative values for $^{2}J$(H5,C6) for all compounds are in qualitative agreement with the experimental values (Table 1). The simulations correctly predict larger magnitudes for the latter coupling constant in

compounds with a galactose residue in the reducing end (**6 – 9**) than in the *gluco*- and *manno*-configured compounds **1 – 5**. The values determined by NMR spectroscopy are −5.8 and −5.4 Hz for compounds **6** and **9**, respectively, similar to the reported values for α-Gal*p*-OMe and β-Gal*p*-OMe, which are −5.2 and −5.5 Hz, respectively.[117] However, these values are lower than at the lowest point of the Karplus equation (−5.3 Hz), indicating that the relationship needs to be revised for compounds having *galacto*-configuration. While the magnitude of the $^{2}J$(H6*R*,H6S) coupling constant is underestimated by at least 1 Hz for all compounds, the additional $^{3}J$(C4,H6*R*) and $^{3}J$(C4,H6*S*) coupling constants (see supporting information Table S1) are in good agreement with the experimental data. The results indicate that the CHARMM36 force field and the newly developed ω parameters satisfactorily reproduce the experimental trends in the rotamer distributions for all the studied compounds. While the new parameters yield a significant improvement over the original parameters there is a slight overestimation of *gg* and underestimation of *tg* rotamer population for **6 – 8**. This could be due to a small limitation in the current parameters or from the TIP3P water model, as solvent influences the relative stabilities of the rotamers in galactopyranosides.[42] Additionally, the populations derived from NMR spectroscopy are expected to have some degree of uncertainty due to errors in the limiting coupling constant values for the three rotamers.[117] The calculated $^{3}J$(H5,H6*R*), $^{3}J$(H5,H6*S*), $^{2}J$(H5,C6) and $^{2}J$(C4,C6) coupling constants and the corresponding populations for compounds **1 – 9** obtained using the ω parameters derived with allowed phase variation are given in supporting information Tables S4 and S5, respectively.

***Conformational Analysis of ω′ Torsion Angles (O5′—C5′—C6′—O6′)***

The two $^{3}J$(H5,H6*R*) and $^{3}J$(H5,H6*S*) values related to the ω′ torsion angle in the non-reducing end residue of disaccharides **1 – 7** are given in Table 1. The calculated values are in good agreement

with the experimental values. However, some minor discrepancies were observed, for instance, for **5** where the differences in experimental and calculated values for $^{3}J$(H5,H6*R*) and $^{3}J$(H5,H6*S*) are > 1.0 Hz. Calculated values for the $^{2}J$(H5,C6) coupling constants are in agreement with the experimental values which are available for compounds **3**, **4** and **6** (see supporting information Table S6). The previously published parameters for the hexopyranose monosaccharides have been reported to slightly overestimate the *tg* rotamer in galactopyranosides.[25] However, the overall performance of the parameters for the O5′—C5′—C6′—O6′ torsion is satisfactory in the CHARMM36 force field, as the model captures the trends from NMR spectroscopy and crystallography, i.e. a preferred equilibrium between *gt* and *gg* over *tg* in gluco- or manno-pyranosides, whereas the favored equilibrium occurs between the *gt* and *tg* rotamers over the *gg* rotamer in galactopyranosides.[117, 119-121]

***Free Energy Maps for α- or β-(1→6)-Linkage Dihedral Angles***

To obtain a detailed understanding of factors that govern specific conformational sampling around glycosidic linkages, 2D free energy maps for the dihedral angles ϕ/ψ and ψ/ω for **1 – 9** where calculated from the HREX simulations, and these are presented in Figures 3 and 4, respectively.

**Table 5.** Populations (%) in conformational regions of the ϕ and ψ torsion angles calculated for **1 – 9** from HREX MD (10 ns).[a]

| Compound | $\phi_{exo}$ | Anti-ϕ | $\psi_{180°}$ | $\psi_{90°}$ | $\psi_{-90°}$ |
|---|---|---|---|---|---|
| **1** | 99.7 | 0.3 | 81.9 | 18.1 | 0.0 |
| **2** | 97.7 | 2.3 | 89.5 | 7.7 | 2.8 |
| **3** | 96.2 | 3.8 | 92.7 | 3.2 | 4.1 |
| **4** | 99.9 | 0.1 | 89.8 | 10.2 | 0.0 |
| **5** | 98.6 | 1.4 | 89.1 | 6.4 | 4.5 |
| **6** | 99.8 | 0.2 | 86.4 | 9.9 | 3.7 |
| **7** | 99.6 | 0.4 | 87.0 | 3.1 | 9.9 |
| **8** | 99.6 | 0.4 | 81.0 | 15.2 | 3.8 |
| **9** | 99.8 | 0.2 | 90.2 | 1.2 | 8.6 |

[a] For $\phi_{exo}$ an exo-anomeric conformation was defined by the region 0° < ϕ < 120° for α-D-/β-L-anomeric compounds **1, 4, 6** and **8** and –120° < ϕ < 0° for β-D-/α-L-anomeric compounds **2, 3, 5, 7** and **9**. For all compounds, the anti-periplanar $\psi_{180°}$ conformation was defined by the regions 120° < ψ < 180° and –180° < ψ < –120°. The $\psi_{90°}$ and $\psi_{-90°}$ conformations were defined by the regions 0° < ψ < 120° and –120° < ψ < 0°, respectively, in the interval –180° to 180°.

Combined analysis of both the ϕ/ψ and ψ/ω free energy maps provides clues regarding the global minimum conformations for **1 – 9** and other accessible conformations in the (1→6)-linkages. For all compounds, ϕ prefers an exo-anomeric conformation with some transitions to higher energy conformations (anti-ϕ) (Figure 3; Table 5), as has previously been observed in a trisaccharide.[122] Slightly larger populations of the anti-ϕ conformations are observed for the β-linked *gluco*-configured disaccharides **2**, **3** and **5** as compared to other disaccharides. For the α-D-/β-L-linked disaccharides **1, 4, 6** and **8**, the ϕ torsion angle adopts values around 70°, while for the β-D-/α-L-linked disaccharides **2**, **3**, **5**, **7** and **9** the values are around −70°. The preference for the exo-anomeric conformation for ϕ was also confirmed by the calculated $^{3}J$(C6,H1′) coupling constants, which are in good agreement with the experimental values (Table 2). However, the experimental observation that this coupling constant is larger in β-linked than in α-linked disaccharides is not reproduced. For all compounds, the anti-periplanar conformation at the ψ torsion angle (i.e., 120º < ψ < 180º or –180º < ψ < –120º; $\psi_{180°}$) was preferred with populations ranging from 80% to 90% (Table 3). In addition, some sampling centered on 90º (0 < ψ < 120; $\psi_{90°}$) or –90º (–120 < ψ < 0; $\psi_{-90°}$) was observed. Although higher in energy in the present study, NMR and molecular modeling studies reported by Lycknert *et al.*[84] showed that conformations with $\psi_{-90°}$ were present upon binding of β-D-Glc*p*NAc-(1→6)-α-D-Man*p*-OMe (**2**) with wheat germ agglutinin (WGA) lectin. The calculated $^{3}J$(C1′,H6*R*) and $^{3}J$(C1′,H6*S*) coupling constants are slightly underestimated as compared to the experimental values in most of the compounds

(Table 3), indicating that the populations of the $\psi_{90^\circ}$ or $\psi_{-90^\circ}$ conformations are slightly larger than in the simulations. From the ψ/ω free energy maps shown in Figure 4 it is clear that all disaccharides show lower energy regions representing three rotamers of ω staggered around 60º (*gt*), –60º (*gg*) or 180º (*tg*). In **1 – 5** there is a preference for lower energy minima located around 60º and –60º while minima at 180º have higher energy. Similarly, for **6 – 9** there is a preference for the two lower energy minima located around 60º and 180º while minima at –60º are also being sampled.

In general, ϕ/ψ and ψ/ω free energy maps for **1 – 9** qualitatively agree with the prior theoretical and experimental observations.[37, 60, 64, 74, 123-124] For instance, Wormald *et al.*[10] reported the crystallographic average of 64.7º ± 10.4º/–178.4º ± 10.0º/–60.3º ± 14.0º (*gg* rotamer) and 67.0º ± 10.5º/178.5º ± 13.7º/66.0º ± 13.8º (*gt* rotamer) for the ϕ/ψ/ω torsion angles in α-D-Man*p*-(1→6)-D-Man*p*. Detailed analysis of the ϕ/ψ and ψ/ω energy maps also provided conformational preferences of ω when ψ deviates from the anti-periplanar conformation. We observe that for all compounds (except for **8**) there is a preference for the *gt* rotamer of ω when ψ adopts $\psi_{90^\circ}$ or $\psi_{-90^\circ}$ conformations, independent of the linkage configuration. For compound **8**, with $\psi_{90^\circ}$ there is a preference for *gt* at ω, while with $\psi_{-90^\circ}$ there is a preference for *tg*. 1D plots of probability distributions of ϕ, ψ and ω for **1 – 9** are shown in Figure S5 of the supporting information.

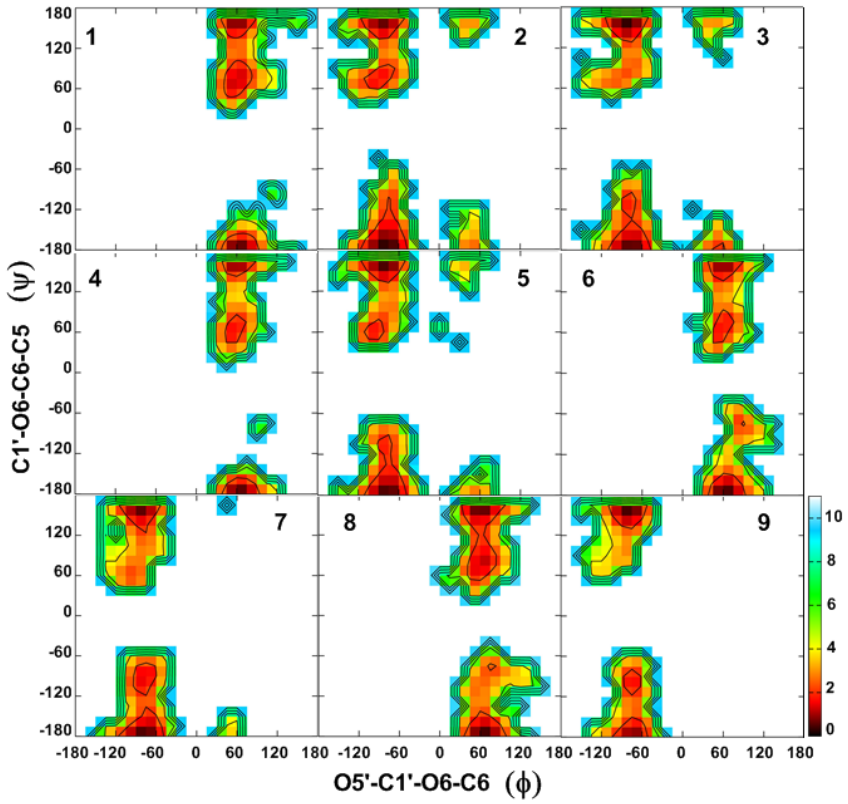


**Figure 3.** Two-dimensional free energy surfaces for the ϕ (O5′—C1′—O6—C6) vs. ψ (C1′—O6—C6—C5) dihedrals for **1 – 9**, given in degrees, calculated from the HREX MD simulations. Free energies are calculated from the natural logarithm of the relative probability and are given in kcal·mol$^{-1}$.

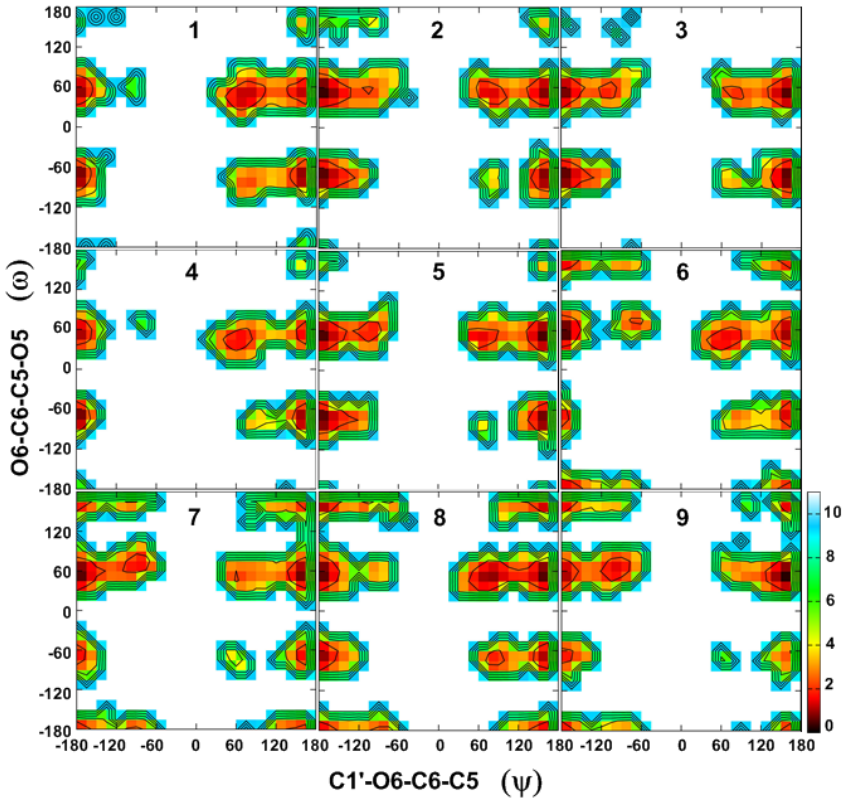


**Figure 4.** Two-dimensional free energy surfaces for the ψ (C1′—O6—C6—C5) vs. ω (O6—C6—C5—O5) dihedrals for **1 – 9**, given in degrees, calculated from the HREX MD simulations. Free energies are calculated from the natural logarithm of the relative probability and are given in kcal·mol$^{-1}$.

***Proton-proton Distances***

Proton-proton distances, *r*(H—H), calculated from NMR cross-relaxation rates and from HREX based explicit solvent MD simulations of compounds **2**, **6** and **8** are given in Table 6. The cross-relaxation rates for compound **2** were available from a previous study.[84] In this study, we measured cross-relaxation rates, shown in Tables S7 and S8 in the Supporting Information, for compounds **6** and **8**, representing disaccharides with *galacto*-configuration in the reducing end residue. A sample spectrum as well as the peak integrals at different mixing times for compound **8** are shown in Figure 5. The effective inter-proton distances for relevant proton pairs were calculated over the MD trajectory as $1/r_{eff}=<r_{MD}^{-6}>^{1/6}$. There is good agreement between calculation and experiment

for the *r*H1′—H6$_{pro\text{-}R}$ values for **2** and for *r*H1′—H6$_{pro\text{-}S}$ in **2**, **6** and **8**. Due to overlapping resonances, some proton-proton distances for **6** and **8** could not be measured. However, the sum of cross-relaxation rates obtained for *r*H1′—H5 and *r*H1′—H6$_{pro\text{-}R}$ in **6** and for *r*H1′—H4 and *r*H1′—H6$_{pro\text{-}R}$ in **8** are in very good agreement with the calculated values. The H1′—H4 distance in compound **6**, as well as H4—H6$_{pro\text{-}S}$ in compound **2**, is overestimated in the new force field.

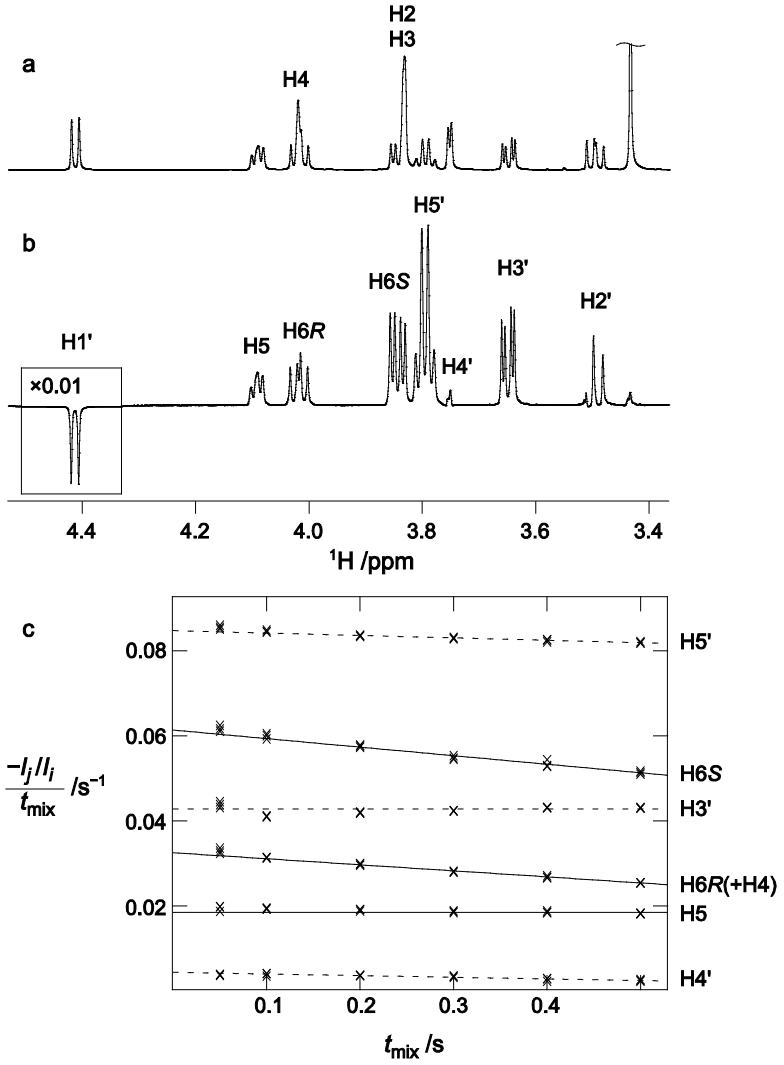


**Figure 5.** Cross-relaxation measurements in compound **8**; (a) 1D $^{1}$H spectrum and (b) 1D $^{1}$H,$^{1}$H SPFGSE NOESY spectrum obtained with excitation at H1' and a 500 ms cross-relaxation delay ($t_{mix}$). (c) Normalized peak integrals divided by $t_{mix}$ for different values of $t_{mix}$ (crosses) together with the fitted equations (lines). Intra- and interresidual interactions are shown as dashed and full lines, respectively.

**Table 6.** Effective proton-proton distances from HREX explicit solvent MD simulations and NMR experiments for disaccharides **2**, **6** and **8**.

| **Compd. 2** | | | **Compd. 6** | | | **Compd. 8** | | |
|---|---|---|---|---|---|---|---|---|
| | $r_{eff}$ /Å | | | $r_{eff}$ /Å | | | $r_{eff}$ /Å | |
| **proton pair** | **MD** | **NMR**[#] | **proton pair** | **MD** | **NMR** | **proton pair** | **MD** | **NMR** |
| | | | H1'-H2'(ref) | 2.41 | 2.42 | H1'-H2'(ref) | 3.06 | 3.00 |
| H1'-H3'(ref) | 2.53 | 2.52 | | | | H1'-H3'(ref) | 2.52 | 2.64 |
| | | | H1'-H4'(ref) | 4.07 | 4.05 | H1'-H4'(ref) | 4.02 | 3.88 |
| H1'-H5'(ref) | 2.32 | 2.33 | | | | H1'-H5'(ref) | 2.32 | 2.35 |
| H1'-H6$_{pro\text{-}R}$ | 2.33 | 2.45 | H1'-H6$_{pro\text{-}R}$+H5* | 2.59 | 2.50 | H1'-H6$_{pro\text{-}R}$+H4* | 2.75 | 2.76 |
| H1'-H6$_{pro\text{-}S}$ | 2.73 | 2.69 | H1'-H6$_{pro\text{-}S}$ | 2.38 | 2.43 | H1'-H6$_{pro\text{-}S}$ | 2.36 | 2.48 |
| H4-H6$_{pro\text{-}S}$ | 3.18 | 2.85 | H4-H6$_{pro\text{-}S}$ | 2.71 | 2.61 | H1'-H5[§] | 3.04 | 3.03 |
| H5-H6$_{pro\text{-}S}$ | 2.48 | 2.22 | H1'-H4[§] | 4.51 | 4.07 | | | |

#Calculated using cross-relaxation rates from Lycknert *et al.*[84]
*Overlapping resonances, only sum of cross-relaxation rates obtained.
§Average of both excitations (H1'→H4/H5 and H4/H5→H1')

To obtain further insight into these discrepancies, probability distributions of the proton-proton distances, *r*H1′—H6$_{pro\text{-}R}$, *r*H1′—H4, *r*H1′—H5 and *r*H4—H6$_{pro\text{-}S}$ were calculated from HREX MD simulations of **2**, **6** and **8** and are given in Figure 6.

As shown in Figure 6a, the *r*H1′–H6$_{pro\text{-}R}$ distribution has mainly two peaks for all three compounds. The effective *r*H1′–H6$_{pro\text{-}R}$ distance is governed by ψ, as shown in plots of ψ versus *r*H1′–H6$_{pro\text{-}R}$ for **2**, **6** and **8** (Figure 7a). The $\psi_{180°}$ population of the α-D-/β-L-(1→6)-linked compounds **6** and **8** have H1′–H6$_{pro\text{-}R}$ distances mostly ranging from 2.5 – 3.5 Å, whereas for the β-D-(1→6)-linked compound **2**, these range from 2.0 – 3.2 Å (Figure 6a). The second peak in the range of >3.2 Å for **2** and of >3.5 Å for **6** and **8** corresponds to the H1′–H6$_{pro\text{-}R}$ distance in the $\psi_{90°}$ conformation. The slightly underestimated H1′–H6$_{pro\text{-}R}$ distance in **2** may be due to under-population of $\psi_{90°}$ conformation. For **2**, there is also a minor contribution from the anti-ϕ conformation with $\psi_{180°}$. Although **6** and **8** sampled minor populations with $\psi_{-90°}$ (Table 5, Figure 7a), the third peak for H1′–H6$_{pro\text{-}R}$ in the range of 2.0 – 2.5 Å is not discernible in Figure 6a, as it overlaps with the contribution from $\psi_{180°}$. Only the sum of the cross-relaxation rates for the H1′–

$H6_{pro\text{-}R}$ and H1′–H5 (**6**) or H1′–H4 (**8**) interactions could be determined. Thus, it is not possible to determine the agreement between experiment and simulation for the individual interactions. However, the sums of the calculated effective distances are in excellent agreement with the experimental values.

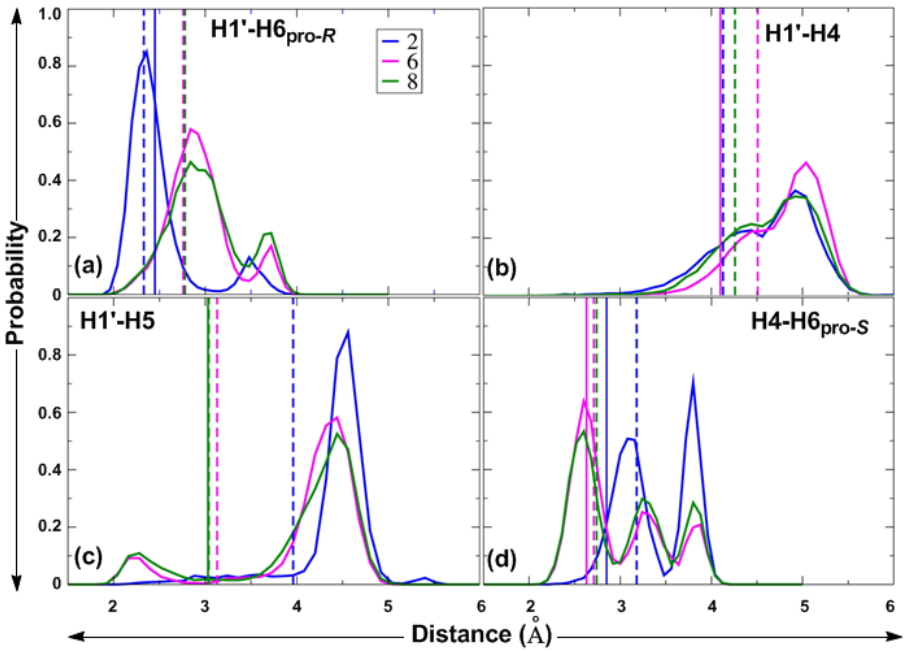


**Figure 6.** Proton-proton distance distributions for **2, 6** and **8** calculated from the HREX MD simulations. *r*H1′,$H6_{pro\text{-}R}$ (a), *r*H1′,H4 (b), *r*H1′,H5 (c) and *r*H4,$H6_{pro\text{-}S}$ (d) are given in Å. Solid spikes represents experimental effective distances and dashed spikes represents effective distances from MD simulations.

The *r*H1′–H4 distribution curves for **6** and **8** (Figure 6b) and the plot of ψ versus *r*H1′–H4 (Figure 7b) show two major peaks around 4.4 and 5.0 Å, representing sampling of all the three $\psi_{180^\circ}$, $\psi_{90^\circ}$ and $\psi_{-90^\circ}$ conformations. However, *r*H1′–H4 is also dependent on the conformational preferences at ω as shown in Table 7. The distribution curves for *r*H1′–H5 (Figure 6c) for **6** and **8** show two major peaks, one around 2.3 Å and a second around 4.3 Å. Plots of ψ versus *r*H1′–H5 (Figure 7c) show that the values of *r*H1′–H5 are around 2.3 Å in the $\psi_{90^\circ}$ conformation and that in the $\psi_{180^\circ}$ conformation, the H1′–H5 distance is longer.

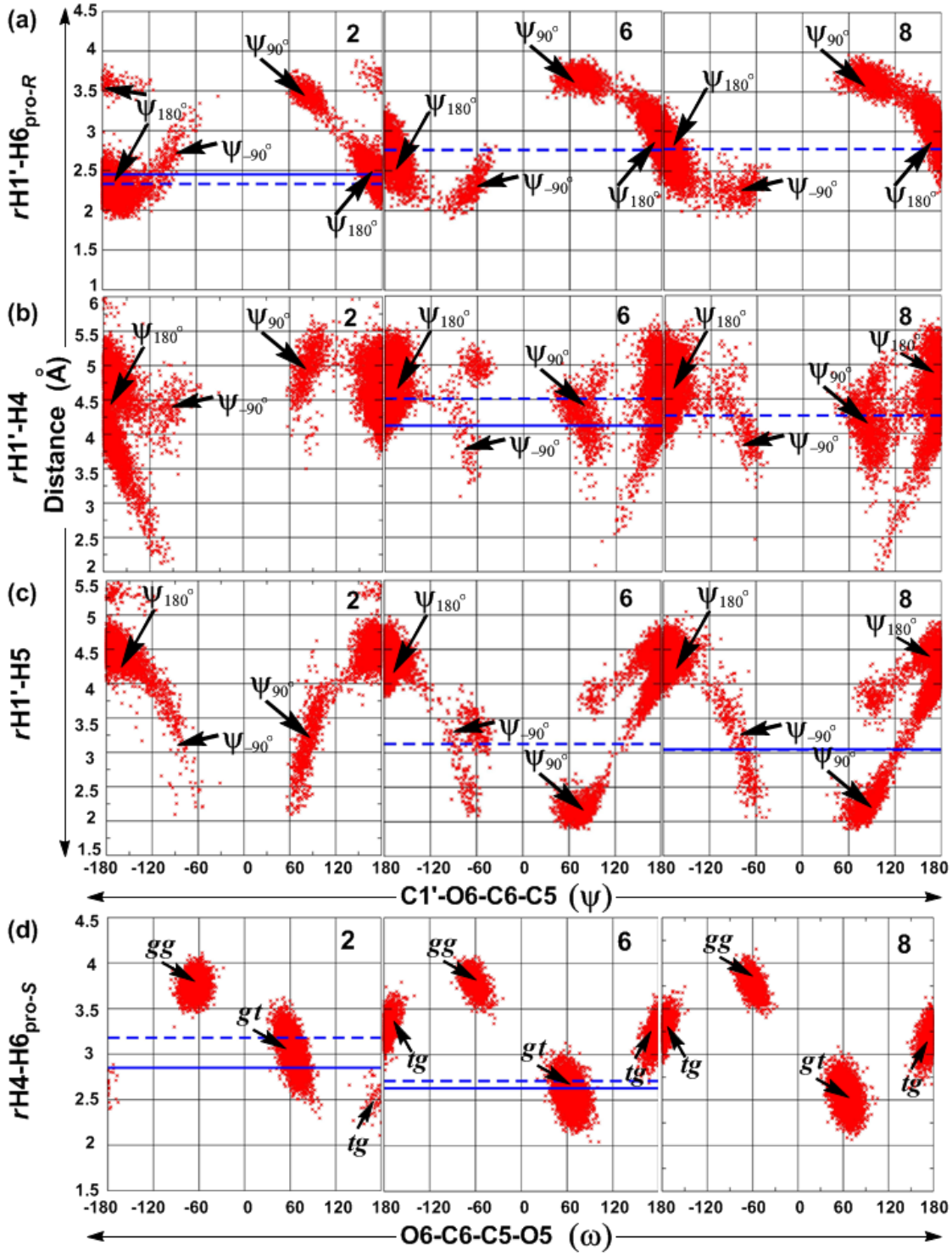


**Figure 7.** ψ vs. *r*H1′–H6$_{pro\text{-}R}$ (a), ψ vs. *r*H1′–H4 (b), ψ vs. *r*H1′–H5 (c) and ω vs. *r*H4–H6$_{pro\text{-}S}$ (d) for **2, 6** and **8** obtained from HREX MD simulations. Proton-proton distances are in Å and dihedral angles in degrees. Solid blue lines represent experimental effective proton-proton distances and dashed blue lines represent calculated effective proton-proton distances.

**Table 7.** Effective proton-proton distances (Å) and the population (%) for each conformational region calculated from aqueous HREX MD simulations for **6** and **8**.

| | **Compd. 6** | | | **Compd. 8** | | |
|---|---|---|---|---|---|---|
| ψ_ω | ***r*H1'-H4** | ***r*H1'-H5** | **%PopMD** | ***r*H1'-H4** | ***r*H1'-H5** | **%PopMD** |
| $\psi_{180°}$_*gt* | 4.88 | 4.11 | 48.2 | 4.78 | 3.99 | 37.5 |
| $\psi_{90°}$_*gt* | 4.16 | 2.17 | 8.9 | 3.97 | 2.23 | 12.6 |
| $\psi_{-90°}$_*gt* | 4.97 | 3.33 | 2.3 | 4.97 | 3.69 | 0.4 |
| $\psi_{180°}$_*gg* | 5.01 | 4.53 | 14.1 | 5.02 | 4.54 | 17.4 |
| $\psi_{90°}$_*gg* | 4.66 | 3.82 | 1.0 | 4.66 | 3.82 | 2.2 |
| $\psi_{-90°}$_*gg* | -[a] | - | 0.0 | 4.07 | 4.58 | 0.0 |
| $\psi_{180°}$_*tg* | 4.12 | 4.39 | 24.1 | 4.05 | 4.39 | 26.1 |
| $\psi_{90°}$_*tg* | 2.30 | 3.65 | 0.0 | 2.38 | 3.75 | 0.4 |
| $\psi_{-90°}$_*tg* | 3.90 | 2.56 | 1.4 | 3.99 | 2.78 | 3.4 |

[a]Absent in the MD simulation.

To facilitate the understanding of the distribution of ψ and ω and the corresponding *r*H1′–H4 and *r*H1′–H5 distances, we calculated effective *r*H1′–H4 and *r*H1′–H5 distances for each of the different conformations of ψ and ω (Table 7). The populations of the conformations in the MD simulations are given in Table 7. For compound **6**, the H1′–H4 distance from simulation, 4.51 Å, is slightly longer than experimental value of 4.07 Å. This may be attributed to under-population of the two conformations in which this distance is short, namely the $\psi_{90°}$_*tg* and $\psi_{-90°}$_*tg* conformations, having effective *r*H1′–H4 distances equal to 2.30 and 3.90 Å, respectively. In addition, over-population of the $\psi_{180°}$_*gg* conformation (14.1 % in **6**) with long *r*H1′–H4 distance (5.01 Å) may have contributed to the overestimation of the *r*H1′–H4 in the simulations. In compound **8**, the $\psi_{90°}$_*gt* and $\psi_{-90°}$_*tg* conformations, for which the effective *r*H1′–H5 distances are 2.23 and 2.78 Å, respectively, are likely adequately sampled as deduced by the excellent agreement between the values from the simulation (3.04 Å) and from NMR spectroscopy (3.03 Å, Table 6).

The two or three peaks in the probability distribution curves of *r*H4–H6$_{pro\text{-}S}$ for compounds **2**, **6** and **8** (Figure 6d) represent the three different rotamers (*gt*, *gg* and *tg*) of ω as deduced from the plots of ω versus *r*H4–H6$_{pro\text{-}S}$ (Figure 7d). The relationship between ω and the H4–H6$_{pro\text{-}S}$ distance depends on the orientation of H4. For compound **2**, which is a *manno*-configured pyranoside, H4 is axially oriented and the effective *r*H4–H6$_{pro\text{-}S}$ distance is short, 2.51 Å, in the *tg* conformation of ω (Figure 7d). The experimental distance of 2.85 Å is consistent with small populations of the *tg* rotamer in **2**. In the *gt* and *gg* rotamers, the effective distances are 3.01 Å and 3.75 Å, respectively. The overestimation of H4–H6$_{pro\text{-}S}$ by approximately 0.3 Å is likely caused by the over-population of *gg* combined with the under-population of the *tg* conformation in compound **2.** For the *galacto*-configured pyranosides in **6** and **8**, with H4 being equatorially oriented, the H4–H6$_{pro\text{-}S}$ distance is short, 2.54 and 2.51 Å, respectively, in the *gt* conformation and longer in the *gg* (3.77 and 3.76 Å, respectively) and *tg* conformations (3.22 and 3.20 Å, respectively). The slight overestimation of the H4–H6$_{pro\text{-}S}$ distance by approximately 0.1 Å in compound **6** reflects the over-population of the *gg* rotamer at the expense of the *tg* rotamer, as compared with the experimental populations shown in Table 4.

***Hydrogen-Bonding Analysis***

Hydrogen bonding interactions were investigated to understand (i) to what extent intramolecular H-bonding is maintained in the aqueous phase and (ii) to what extent water-mediated intermolecular interactions play a role in determining distributions of ω in oligosaccharides. In addition to the type of sugar involved in the (1→6)-linkage, it is also important to investigate any role of anomeric differences in the water-mediated intermolecular H-bonding pattern and how these affect the conformational sampling. For this purpose, the intramolecular H-bonds in the

disaccharides were analyzed in terms of intra-residue and inter-residue H-bonds. The H-bond occupancies from the HREX simulations of **1** – **9** are summarized in Table 8.

Intra-residue H-bonds are characteristic of the residue type, for instance, **1**, **2** and **3** with mannopyranoside as the reducing end residue favor the O2· · ·HO3 and O3· · ·HO2 intra-residue H-bonds, as well as the corresponding interactions in the terminal mannosyl residue in **1**, while other intra-residue H-bonds were almost absent (Table 8). In **4** and **5**, where glucopyranose is present as the reducing end residue and in **3**, **4** and **6**, where it is the non-reducing residue, the O3· · ·HO2 intra-residue H-bond is present to approximately the same extent as for the mannopyranoses whereas the occupancies of the O2· · ·HO3 H-bonds are lower. The difference between manno- and glucopyranosides is attributed to the relative orientations of hydroxyls at positions C2 and C3 which are in axial-equatorial and equatorial-equatorial arrangements in the respective sugars. Moreover, for gluco- and mannopyranoside residues, the equatorial orientation of the hydroxyl at position C4 disfavors intra-residue H-bonds involving either of the O4 or HO4 atoms, as seen for compounds **1** – **5** (Table 8). Conversely, the axial orientation of the C4 hydroxyl in the galactopyranoside units found at the reducing end in **6 - 9** and at the non-reducing end in **5** leads to relatively higher occupancies for intra-residue H-bonds involving the C3 and C4 hydroxyl groups (O4· · ·HO3, O6· · ·HO4 and O4· · ·HO6, Table 8). In contrast to the gluco- and mannopyranosides, where the C4 hydroxyl loses its intra-residue H-bonds in the presence of water, the galactopyranosides in **6** – **9** maintain the intra-sugar H-bonds (O6· · ·HO4 and O4· · ·HO3) to a small extent.

In the absence of solvent, intra-residue H-bonding involving the C4 hydroxyl stabilizes the ω rotamer in which O4 and O6 are close to each other, that is, *tg* or *gg* in the cases of an equatorial or axial hydroxyl at C4, respectively.[42, 117] However, competing H-bonding with water diminishes

the importance of these H-bonds in aqueous solution and consequently the repulsive interactions dominate, leading to the small populations typically observed for these rotamers.[42]

Thus, although H-bonding between O6· · ·HO4 is present to a large extent in the *tg* rotamer for compounds **1** – **5** with an equatorial C4 hydroxyl, the population of this rotamer is small in these compounds. Furthermore, the populations of the *tg* rotamer is similarly small in compounds **1** – **5**, although compounds **1** – **3** have larger occupancies of the O6· · ·HO4 H-bond in the *tg* rotamer than do compounds **4** and **5**. Similarly, for compounds **6** – **9** having a galactose residue in the reducing end, O6· · ·HO4 H-bonding is present to a large extent for the *gg* rotamer. However, the differences in the populations of the *gg* rotamer within this group do not correlate with the minor differences observed in the extent of O6· · ·HO4 H-bonding in this rotamer. Thus, differences in the strength of the O6· · ·HO4 H-bond are likely having a negligible influence on the rotameric distribution at the ω torsion angle in aqueous solutions in all of the studied compounds.

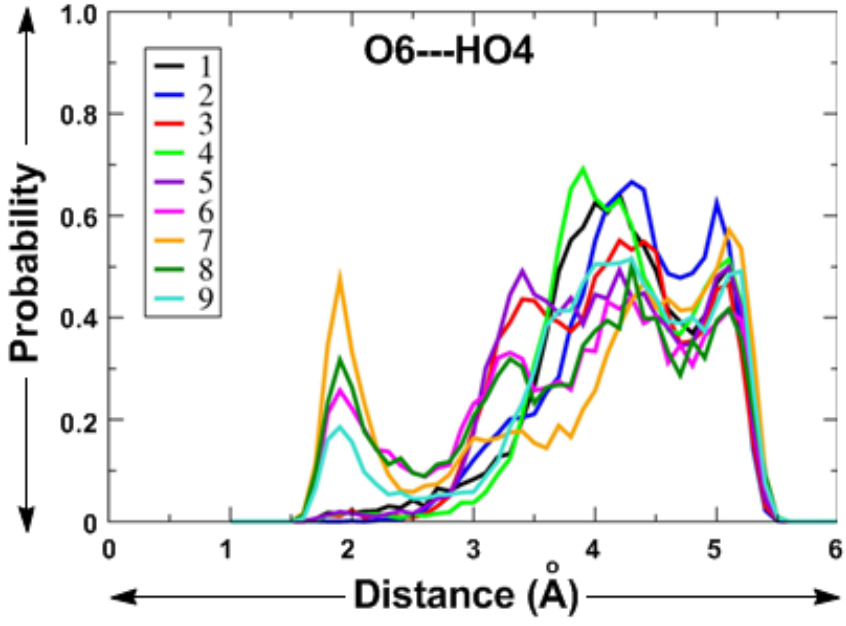


**Figure 8.** Distance probability distribution for the O6· · ·HO4 distance in **1** – **9** obtained from HREX MD simulations.

The distance probability distribution plots for the O6· · ·HO4 distance in **1 – 9** (Figure 8) show that for **1 – 5**, this distance is >3 Å while for **6 – 9** there is a significant probability density below 2.5 Å (with lesser probability density for **9**). This indicates that the O6· · ·HO4 intra-sugar H-bond can, to some extent, compete with the individual interactions with water.

Inter-residue H-bonding between the two monosaccharide units in **1 – 9** is absent in most of the disaccharides. This is consistent with the observation made by Perić-Hassler *et al.*[74] for two (1→6) linked disaccharides, isomaltose and gentiobiose. However, H-bonding was observed in the present study between the linking oxygen, O6, and HO2′ in **4** (18.8%), **6** (14.2%) and **9** (19.7%), i.e., in all of the α-linked compounds except for compound **1** in which O2′ is axially oriented. Calculations of water radial distribution functions in **1 – 9** (Figure 9) show a decrease in water occupancy around the O6 atom (Figure 9a) compared to around the O6′ atom (Figure 9b). This is largely due to the increased steric hindrance in the former case compared to the hydroxymethyl O6′ atom. The decreased accessibility of water to the O6 atom is likely the reason for the inability of water to compete with the intramolecular O6 – HO4 H-bond (*vide supra*).

Interestingly, there are pronounced differences in the region around 3 Å in the Ow–O6 RDFs as shown in Figure 9a, with the β-linked compounds (**2**, **3**, **5**, **7** and **8**) having higher densities than the α-linked compounds (**1**, **4**, **6** and **9**). This difference indicates that the O6 atom in a β-(1→6)-linkage is more exposed to the solvent than the corresponding atom in an α-(1→6)-linkage.

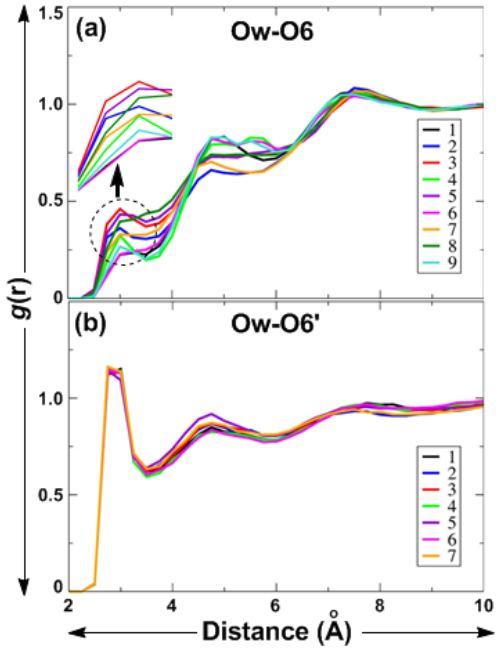


**Figure 9.** (a) Radial distribution functions for Ow (water oxygen) and O6. (b) Radial distribution functions for Ow and O6′. Note that O6′ is in the terminal end sugar and O6 participates in the (1→6)-glycosidic linkage.

The role of bridging water molecules in the function and structural stability of carbohydrates has been extensively reported.[125-126] The probabilities of such bridging water molecules between the two residues which may have influenced the distributions of ω in gluco-, manno- and galactopyranosides are summarized in Table 9. For compounds **1 – 5,** with gluco- and mannopyranosides at the reducing end, both the *gg* and *gt* conformations allow water to simultaneously form an H-bond to one of the ring oxygens (O5 or O5′) and the linkage oxygen O6 atom (Figures 10a and 10b). Occasionally, there are cases where water simultaneously forms H-bonds to the ring oxygen of both monosaccharide units (Figure 10c), as has previously been observed in crystal structures.[127] Such water-mediated interactions between two monosaccharide units was not observed in the *tg* conformation in any of the compounds. For compounds **7 – 9**, the *gt* rotamer is associated with the water-mediated O5· · ·O6 (**8** and **9**) and O5'· · ·O6 (**7** and **8**) interactions. Interestingly, the O5· · ·O6 water-mediated interaction was absent for compounds **6**

and **7** which have D-configuration at the terminal end, in contrast to the two other compounds (**8** and **9**) with a galactose residue at the reducing end, which both have L-configured residues at the non-reducing end. The presence of the water-mediated O6· · ·O5′ and O5· · ·O5′ interactions was found to be higher for the β-linked compounds **2**, **3**, **5**, **7** and **8** than for the other compounds which are α-linked and in which these interactions are virtually absent (Table 9). However, for **6** neither of the ring oxygens (O5 or O5′) was found to interact with the O6 atom via a water bridge. In **2**, water-mediated O6· · ·O=C (carbonyl oxygen) interactions may provide additional stabilization to the *gt* rotamer, as deduced by its greater population as compared to compound **3.**

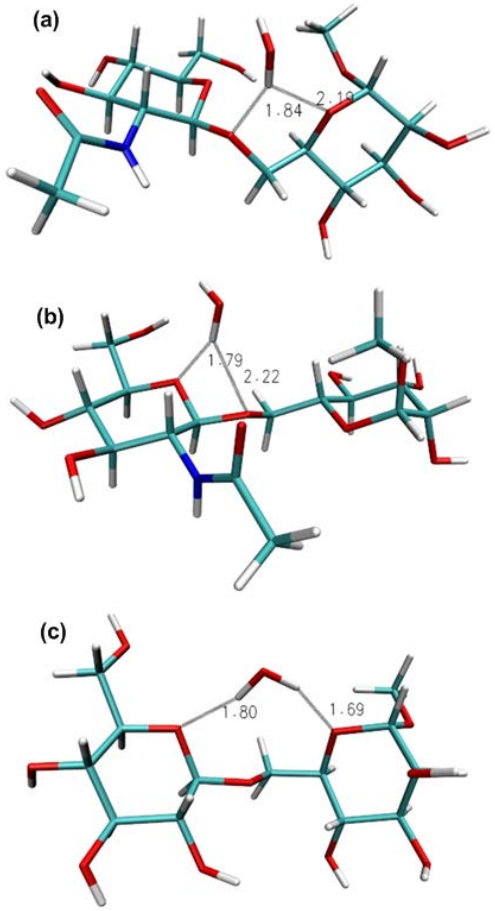


**Figure 10.** Representative snapshots from the HREX simulations of **2** and **3** showing bridging water molecules. (a) In **2**, the *gt* conformation at ω allows water to simultaneously form an H-bond to ring oxygen O5 and linkage oxygen O6 atom, (b) in **2**, the *gt* conformation allows a water bridge between the ring oxygen O5′ and the linkage oxygen O6 atom and (c) in **3**, the *gg* conformation allows a water bridge between the two ring oxygen atoms O5 and O5′.

**Table 8.** Intra-residue hydrogen bond occupancies for **1 – 9** obtained from HREX simulations.

| Compound | *O*-methyl glycoside | | | | Terminal residue | | | | |
|---|---|---|---|---|---|---|---|---|---|
| | **O2···HO3** | **O3···HO2** | **O4···HO3** | **O6···HO4** | **O2'···HO3'** | **O3'···HO2'** | **O4'···HO3'** | **O6'···HO4'** | **O5'···HO6'** |
| **1** | 0.21 | 0.12 | 0.05 | - | 0.19 | 0.11 | 0.05 | 0.01 | 0.19 |
| **2** | 0.20 | 0.12 | 0.06 | 0.00 | - | - | 0.04 | 0.01 | 0.16 |
| **3** | 0.20 | 0.11 | 0.06 | - | 0.07 | 0.10 | 0.05 | 0.01 | 0.15 |
| **4** | 0.07 | 0.10 | 0.04 | 0.01 | 0.08 | 0.10 | 0.05 | 0.01 | 0.18 |
| **5** | 0.07 | 0.10 | 0.05 | - | 0.07 | 0.09 | 0.22 | 0.01 | 0.06 |
| **6** | 0.07 | 0.10 | 0.24 | 0.11 | 0.07 | 0.11 | 0.06 | 0.02 | 0.16 |
| **7** | 0.06 | 0.11 | 0.24 | 0.09 | - | - | 0.04 | 0.01 | 0.13 |
| **8** | 0.06 | 0.12 | 0.25 | 0.15 | 0.01 | 0.10 | 0.27 | - | - |
| **9** | 0.06 | 0.12 | 0.21 | 0.04 | 0.06 | 0.10 | 0.26 | - | - |

Hydrogen bonding occupancies based on a distance cutoff of 2.5 Å between the H-bond donors and acceptors.

**Table 9.** Water bridge occupancies for **1 – 9** obtained from HREX simulations.[a]

| Compound | **O5···O6** | **O6···O5'** | **O5···O5'** | **O5···O2'** | **O5···HO2'** | **O6···O2'** | **HO4···O2'** | **O6···O=C** |
|---|---|---|---|---|---|---|---|---|

| | | | | | | | | |
|---|---|---|---|---|---|---|---|---|
| **1** | 0.25 | - | 0.00 | - | - | - | - | - |
| **2** | 0.30 | 0.18 | 0.08 | - | - | - | - | 0.15 |
| **3** | 0.41 | 0.19 | 0.11 | 0.16 | - | 0.17 | 0.11 | - |
| **4** | 0.29 | - | 0.00 | 0.26 | 0.25 | 0.22 | - | - |
| **5** | 0.32 | 0.18 | 0.11 | 0.13 | - | 0.14 | 0.11 | - |
| **6** | - | - | 0.00 | - | - | 0.15 | - | - |
| **7** | - | 0.18 | 0.02 | - | - | - | - | 0.11 |
| **8** | 0.26 | 0.15 | 0.11 | - | - | 0.14 | - | - |
| **9** | 0.26 | - | 0.00 | 0.22 | 0.17 | 0.24 | - | - |

[a]H-bond occupancies of >0.08 are shown. The BRIDge option in CHARMM was used for calculating the average number of water bridges formed between selected pairs of atoms.

***Conformational Analysis of the ω Torsion Angle in the Trisaccharide α-Neu5Ac-(2→6)-β-D-Galp-(1→4)-β-D-Glcp-OEtN$_3$***

Having confidence in the ability of the force field to reproduce conformational distributions around α- or β-(1→6)-linked *gluco*-, *manno*- and *galacto*-configured disaccharides (**1 – 9**), we extended HREX-MD simulation to the trisaccharide α-Neu5Ac-(2→6)-β-D-Gal*p*-(1→4)-β-D-Glc*p*-OEtN$_3$ (**10**). It consists of an *N*-acetylated derivative of neuraminic acid (also known as sialic acid) linked to β-D-galactopyranoside by an α-(2→6)-linkage. *N*-Acetylneuraminic acid (Neu5Ac) is often a terminal unit in glycoproteins and glycolipids that play important roles in a variety of biochemical processes. A few NMR-based studies have been undertaken to determine the preferred conformation about α-Neu5Ac-(2→6) linkages.[128-130,131]

Analysis of the HREX simulation yielded calculated $^3J$(H5,H6*R*) and $^3J$(H5,H6*S*) values of 7.82 Hz and 4.29 Hz, respectively, for compound **10**. These are in good agreement with the experimental values, being 8.39 Hz and 3.85 Hz, respectively. They are also similar to experimental values for the disaccharide α-Neu5Ac-(2→6)-β-D-Gal*p*-OMe reported by Ohuri *et al.*,[132] viz. 7.60 Hz and 4.60 Hz for $^3J$(H5,H6*R*) and $^3J$(H5,H6*S*), respectively. The calculated value of −3.19 Hz for the $^2J$(H5,C6) coupling constant is underestimated compared to the experimental value (−5.4 Hz), as was observed also for compounds **5 – 9** (Table 1). The calculated population distribution for ω in **10** was 66:6:28 for the *gt*/*gg*/*tg* rotamers, in excellent agreement with the experimentally determined population distribution which was 73:2:25.

The $^3J$(C1′,H6*R*) and $^3J$(C1′,H6*S*) coupling constants calculated from the simulation were 2.58 and 1.65 Hz, respectively, in excellent agreement with the values from NMR spectroscopy, viz. 2.47 and 1.64 Hz, respectively. These values are smaller than the corresponding values for compounds **1 – 9**, indicating that the conformational distribution with respect to the ψ torsion angle

in **10** is different from that in compounds **1** – **9**. This is also observed in the MD simulation, that unlike in **1** – **9**, populates the antiperiplanar conformation at the ψ torsion angle to 99% while $\psi_{90°}$ and $\psi_{-90°}$ contribute only 1%. Interestingly, inter-residue H-bonding was observed between oxygen O3 of β-D-Glc*p* and HO7′ of α-Neu5Ac (19%) as shown in Figure 11, which occurs in an overall bended conformation in which the terminal residue and non-reducing end residue come close. A similar, folded conformation has previously been observed in the complex formed between α-Neu5Ac-(2→6)-β-D-Gal*p*-(1→4)-D-Glc*p* and the HA70 hemagglutinin of botulinum toxin.[133] As for the other compounds having an equatorial linkage, i.e. the β-linked compounds **2**, **3**, **5**, **7** and **8** (Table 9), for **10** the ring oxygen (O6′) interacts with the linkage O6 oxygen atom via a water bridge, being present to 24%. Furthermore, there were other water mediated interactions observed at the α-(2→6)-linkage, between O6· · ·HO7′ (10%) as well as between O6 and the two oxygen atoms in the carboxylic acid group in the Neu5Ac residue (~11% in each case).

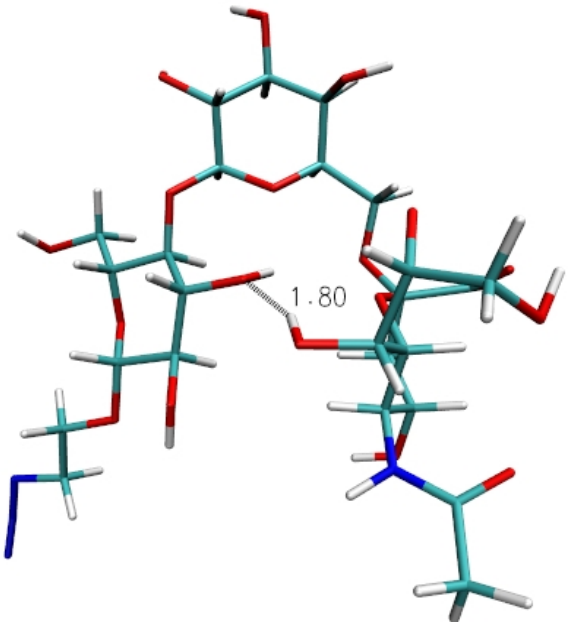


**Figure 11.** Molecular model of compound **10** showing H-bonding between O3 in the reducing end glucose residue and HO7′ in the terminal end Neu5Ac residue.

**Conclusions**

In the present study, the conformational dynamics of α- or β-(1→6)-linked *gluco*-, *manno*- and *galacto*-configured oligosaccharides (**1 – 10**) have been explored using HREX-MD simulations and NMR spectroscopy. The three bonds that comprise the (1→6)-linkage showed the least flexibility for ϕ, which prefers the exo-anomeric conformation and intermediate flexibility for ψ, which prefers the anti-periplanar conformation ($\psi_{180°}$) with excursions to the $\psi_{90°}$/$\psi_{-90°}$ conformations. The largest conformational fluctuations were observed for ω, with three main rotamers (*gt*, *gg* and *tg*) being sampled. Discrepancies due to the force field were recognized by comparing with experimental *J* coupling constants and proton-proton distances, as well as with populations of the rotamers at the ω torsion angle (*gt*:*gg*:*tg*) deduced from NMR spectroscopy. This prompted us to further optimize the O6—C6—C5—O5 (ω torsion) and O6—C6—C5—C4 parameters, resulting in a revised force field which was shown to accurately predict the rotamer distributions in all of the studied compounds. However, a small limitation was observed in terms of a slight overestimation of *gg* rotamer populations for **2**, **6** and **8** leading to a slight overestimation of the H4–$H6_{pro\text{-}S}$ distances as compared to the experimental measurements for compounds **2** and **6**. This could be due to either the current parameters or from the TIP3P water model used during the simulations, as solvent plays a major role in the relative stabilities of the three ω rotamers. The slight overestimation of *r*H1′–H4 in **6** is likely caused by under-population of the $\psi_{90°}$*_tg* and $\psi_{-90°}$*_tg* conformations.

Direct intramolecular H-bonds between the two monosaccharide units was absent in most of the compounds, although O6· · ·HO2′ H-bonding was observed in the α-(1→6)-linked compounds **4**, **6** and **9**. The diminished importance of intramolecular hydrogen bonding in aqueous solution results in an equilibrium between the *gt* and *gg* rotamers at the ω torsion angle for the gluco- and mannopyranoside-based disaccharides **1** – **5**, as predicted by consideration of the

*gauche* effect and the repulsive interactions between O4 and O6 in the *tg* conformer. Conversely, galactopyranoside-based oligosaccharides show population distributions in equilibrium between the *gt* and *tg* rotamers, as predicted by considering steric interactions disfavoring the *gg* rotamer and the decreased importance of the stabilizing O6···HO4 hydrogen bond in aqueous solutions. Water radial distribution functions, $g(r)$, indicated that the accessibility for water to interact with O6, which is involved in the (1→6)-linkage, is reduced compared to the O6' atom in the terminal residue, as expected due to steric effects.

In conclusion, the herein developed parameters for the ω torsion angle allow more accurate MD simulations to be performed for (1→6)-linked oligosaccharides. The CHARMM36 force field and the newly developed ω parameters reproduce the experimental trends in rotamer distributions for the disaccharides as well as the trisaccharide incorporated in this study. Although the new parameters show a significant improvement over the original parameters there is small limitation evident in terms of a slight overestimation of the *gg* populations and underestimation of the *tg* rotamer populations for *galacto*-configured disaccharides. This could be caused by a small limitation in the current carbohydrate parameters or from the TIP3P water model, as solvent plays a major role in diminishing the importance of the O6···HO4 hydrogen bond as a stabilizing factor for the *gg* rotamer in galactopyranosides. It was also noted that the population distribution for ω in the (2→6)-linked *galacto*-configured trisaccharide did not show as much overpopulation of *gg* as in the *galacto*-configured disaccharides in the study. Furthermore, the small $^{3}J$(C1',H6*R*/*S*) values with excellent agreement between experiment and simulation support the ψ torsion angle assuming an anti-periplanar conformation as its major conformational state at the (2→6)-linkage in trisaccharide **10**.

**Acknowledgement**

A.D.M. would like to thank the National Institutes of Health (NIH) for financial support (GM051501, GM070855) and G.W. would like to thank the Swedish Research Council and the Knut and Alice Wallenberg foundation for financial support.

**Supporting Information**

Additional $^{2}J$ and $^{3}J$ coupling constants associated with ω from experiments and HREX MD simulations using the new C36 parameters (Table S1); $^{2}J$ and $^{3}J$ coupling constants from original C36 parameters using standard MD (Table S2) and HREX MD (Table S3); $^{2}J$ and $^{3}J$ coupling constants (Table S4) and ω torsion population distributions (Table S5) calculated using ω parameters obtained from phase variation; additional $^{2}J$ coupling constants associated with ω′ (Table S6); experimental cross-relaxation rates for compounds **6** (Table S7) and **8** (Table S8); examples of ψ/ω MM free energy surfaces; QM and MM energy scan for ω; comparative time series obtained for the ω torsion angle using the original C36 and new C36 ω parameters. This material is available free of charge via the Internet at http://pubs.acs.org.

**References**

1. Dwek, R. A., Glycobiology: Toward Understanding the Function of Sugars. *Chem. Rev.* **1996,** *96*, 683-720.
2. Dwek, R. A.; Butters, T. D., Introduction: Glycobiology – Understanding the Language and Meaning of Carbohydrates. *Chem. Rev.* **2002,** *102*, 283-284.
3. El Kadib, A.; Bousmina, M., Chitosan Bio-Based Organic–Inorganic Hybrid Aerogel Microspheres. *Chem. Eur. J.* **2012,** *18*, 8264-8277.
4. Koutsopoulos, S., Molecular Fabrications of Smart Nanobiomaterials and Applications in Personalized Medicine. *Adv. Drug Del. Rev.* **2012,** *64*, 1459-1476.
5. Slaney, A. M.; Wright, V. A.; Meloncelli, P. J.; Harris, K. D.; West, L. J.; Lowary, T. L.; Buriak, J. M., Biocompatible Carbohydrate-Functionalized Stainless Steel Surfaces: A New Method for Passivating Biomedical Implants. *ACS Appl. Mater. Interfaces* **2011,** *3*, 1601-1612.
6. Sun, G.; Mao, J. J., Engineering Dextran-Based Scaffolds for Drug Delivery and Tissue Repair. *Nanomedicine* **2012,** *7*, 1771-1784.
7. Alonso, D. M.; Wettstein, S. G.; Dumesic, J. A., Bimetallic Catalysts for Upgrading of Biomass to Fuels and Chemicals. *Chem. Soc. Rev.* **2012,** *41*, 8075-8098.

8. He, Y.; Bagley, D. M.; Leung, K. T.; Liss, S. N.; Liao, B-Q., Recent Advances in Membrane Technologies for Biorefining and Bioenergy Production. *Biotechnol. Adv.* **2012,** *30*, 817-858.
9. Markou, G.; Angelidaki, I.; Georgakakis, D., Microalgal Carbohydrates: An Overview of the Factors Influencing Carbohydrates Production, and of Main Bioconversion Technologies for Production of Biofuels. *Appl. Microbiol. Biotechnol.* **2012,** *96*, 631-645.
10. Wormald, M. R.; Petrescu, A. J.; Pao, Y-L.; Glithero, A.; Elliott, T.; Dwek, R. A., Conformational Studies of Oligosaccharides and Glycopeptides: Complementarity of NMR, X-ray Crystallography, and Molecular Modelling. *Chem. Rev.* **2002,** *102*, 371-386.
11. Lutteke, T.; Frank, M.; von der Lieth, C. W., Data Mining the Protein Data Bank: Automatic Detection and Assignment of Carbohydrate Structures. *Carbohydr. Res.* **2004,** *339*, 1015-1020.
12. Lutteke, T.; Frank, M.; von der Lieth, C. W., Carbohydrate Structure Suite (CSS): Analysis of Carbohydrate 3D Structures Derived from the PDB. *Nucleic Acids Res.* **2005,** *33*, D242-D246.
13. Widmalm, G., A Perspective on the Primary and Three-Dimensional Structures of Carbohydrates. *Carbohydr. Res.* **2013,** *378*, 123-132.
14. Rao, V. S. R.; Qasba, P. K.; Balaji, P. V.; Chandrasekaran, R., *Conformation of Carbohydrates*. Harwood Academic: Amsterdam, The Netherlands, 1998.
15. Duus, J. Ø.; Gotfredsen, C. H.; Bock, K., Carbohydrate Structural Determination by NMR Spectroscopy: Modern Methods and Limitations. *Chem. Rev.* **2000,** *100*, 4589-4614.
16. Bock, K.; Duus, J. Ø., A Conformational Study of Hydroxymethyl Groups in Carbohydrates Investigated by $^{1}$H-NMR Spectroscopy. *J. Carbohydr. Chem.* **1994,** *13*, 513-543.
17. Bose, B.; Zhao, S.; Stenutz, R.; Cloran, F.; Bondo, P. B.; Bondo, G.; Hertz, B.; Carmichael, I.; Serianni, A. S., Three-Bond C-O-C-C Spin-Coupling Constants in Carbohydrates: Development of a Karplus Relationship. *J. Am. Chem. Soc.* **1998,** *120*, 11158-11173.
18. Damm, W.; Frontera, A.; Tirado–Rives, J.; Jorgensen, W. L., OPLS All-Atom Force Field for Carbohydrates. *J. Comput. Chem.* **1997,** *18*, 1955-1970.
19. de Bruyn, A.; Anteunis, M.; de Gussem, R.; Dutton, G. G. S., $^{1}$H-N.m.r. Study of L-Rhamnose, Methyl α-L-Rhamnopyranoside, and 4-*O*-β-D-Galactopranosyl-L-Rhamnose in Deuterium Oxide. *Carbohydr. Res.* **1976,** *47*, 158-163.
20. Hoffmann, M.; Rychlewski, J., Effects of Substituting a OH Group by a F Atom in D-Glucose. Ab Initio and DFT Analysis. *J. Am. Chem. Soc.* **2001,** *123*, 2308-2316.
21. Hori, H.; Nishida, Y.; Ohrui, H.; Meguro, H., Conformational Analysis of Hydroxymethyl Group of D-Mannose Derivatives Using (6*S*)- and (6*R*)-(6-$^{2}H_{1}$)-D-Mannose. *J. Carbohydr. Chem.* **1990,** *9*, 601-618.
22. Molteni, C.; Parrinello, M., Glucose in Aqueous Solution by First Principles Molecular Dynamics. *J. Am. Chem. Soc.* **1998,** *120*, 2168-2171.
23. Senderowitz, H.; Parish, C.; Still, W. C., Carbohydrates: United Atom AMBER* Parameterization of Pyranoses and Simulations Yielding Anomeric Free Energies. *J. Am. Chem. Soc.* **1996,** *118*, 2078-2086.
24. Spieser, S. A. H.; van Kuik, J. A.; Kroon-Batenburg, L. M. J.; Kroon, J., Improved Carbohydrate Force Field for GROMOS: Ring and Hydroxymethyl Group Conformations and Exo-Anomeric Effect. *Carbohydr. Res.* **1999,** *322*, 264-273.

25. Guvench, O.; Greene, S. N.; Kamath, G.; Brady, J. W.; Venable, R. M.; Pastor, R. W.; MacKerell, A. D., Jr., Additive Empirical Force Field for Hexopyranose Monosaccharides. *J. Comput. Chem.* **2008,** *29*, 2543-2564.
26. Roslund, M. U.; Tähtinen, P.; Niemitz, M.; Sjöholm, R., Complete Assignments of the $^{1}H$ and $^{13}C$ Chemical Shifts and $J_{H,H}$ Coupling Constants in NMR Spectra of D-Glucopyranose and All D-Glucopyranosyl-D-Glucopyranosides. *Carbohydr. Res.* **2008,** *343*, 101-112.
27. Church, T.; Carmichael, I.; Serianni, A. S., Two-Bond $^{13}C$-$^{13}C$ Spin-Coupling Constants in Carbohydrates: Effect of Structure on Coupling Magnitude and Sign. *Carbohydr. Res.* **1996,** *280*, 177-186.
28. Barrows, S. E.; Storer, J. W.; Cramer, C. J.; French, A. D.; Truhlar, D. G., Factors Controlling Relative Stability of Anomers and Hydroxymethyl Conformers of Glucopyranose. *J. Comput. Chem.* **1998,** *19*, 1111-1129.
29. Nóbrega, C.; Vázquez, J. T., Conformational Study of the Hydroxymethyl Group in α- D-Mannose Derivatives. *Tetrahedron: Asymmetry* **2003,** *14*, 2793-2801.
30. Brown, J. W.; Wladkowski, B. D., Ab Initio Studies of the Exocyclic Hydroxymethyl Rotational Surface in α-D-Glucopyranose. *J. Am. Chem. Soc.* **1996,** *118*, 1190-1193.
31. Tvaroska, I.; Carver, J. P., Ab Initio Molecular Orbital Calculation of Carbohydrate Model Compounds. 6. The Gauche Effect and Conformations of the Hydroxymethyl and Methoxymethyl Groups. *J. Phys. Chem. B* **1997,** *101*, 2992-2999.
32. Tvaroska, I.; Taravel, F. R.; Utille, J. P.; Carver, J. P., Quantum Mechanical and NMR Spectroscopy Studies on the Conformations of the Hydroxymethyl and Methoxymethyl Groups in Aldohexosides. *Carbohydr. Res.* **2002,** *337*, 353-367.
33. de Vries, N. K.; Buck, H. M., Different Rotamer Populations around the C5-C6 Bond for α- and β-D-Galactopyranosides through the Combined Interaction of the Gauche and Anomeric Effects: A 300-MHz $^{1}H$-N.M.R. and MNDO Study. *Carbohydr. Res.* **1987,** *165*, 1-16.
34. Nishida, Y.; Ohrui, H.; Meguro, H., $^{1}H$-NMR Studies of (6*R*)- and (6*S*)-Deuterated D-Hexoses: Assignment of the Preferred Rotamers About C5-C6 Bond of D-Glucose and D-Galactose Derivatives in Solutions. *Tetrahedron Lett.* **1984,** *25*, 1575-1578.
35. Ohrui, H.; Nishida, Y.; Higuchi, H., The Preferred Rotamer About the C5 -C6 Bond of D-Galactopyranoses and the Stereochemistry of Dehydrogenation by D-Galactose Oxidase. *Can. J. Chem.* **1987,** *65*, 1145-1153.
36. Marchessault, R. H.; Perez, S., Conformations of the Hydroxymethyl Group in Crystalline Aldohexopyranoses. *Biopolymers* **1979,** *18*, 2369-2374.
37. Olsson, U.; Sawen, E.; Stenutz, R.; Widmalm, G., Conformational Flexibility and Dynamics of Two (1→6)-Linked Disaccharides Related to an Oligosaccharide Epitope Expressed on Malignant Tumour Cells. *Chem. Eur. J.* **2009,** *15*, 8886-8894.
38. Epiotis, N. D.; Sarkanen, S.; Bjorkquist, D.; Bjorkquist, L.; Yates, R., Open Shell Interactions, Nonbonded Attraction, and Aromaticity. Implications for Regiochemistry. *J. Am. Chem. Soc.* **1974,** *96*, 4075-4084.
39. Wiberg, K. B.; Murcko, M. A.; Laidig, K. E.; MacDougall, P. J., Origin of the Gauche Effect in Substituted Ethanes and Ethenes. *J. Phys. Chem.* **1990,** *94*, 6956-6959.
40. Pinto, B. M.; Leung, R. Y. N., The Anomeric Effect and Associated Stereoelectronic Effects. Thatcher, G. R. J., Ed. Am. Chem. Soc. Washington, D. C.: 1993; pp 126 - 155.
41. Wolfe, S., The Gauche Effect. Stereochemical Consequences of Adjacent Electron Pairs and Polar Bonds. *Acc. Chem. Res.* **1972,** *5*, 102-111.

42. Kirschner, K. N.; Woods, R. J., Solvent Interactions Determine Carbohydrate Conformation. *Proc. Natl. Acad. Sci. U. S. A.* **2001,** *98*, 10541-10545.
43. Engelsen, S. B.; Monteiro, C.; de Penhoat, C. H.; Perez, S., The Diluted Aqueous Solvation of Carbohydrates as Inferred from Molecular Dynamics Simulations and NMR Spectroscopy. *Biophys. Chem.* **2001,** *93*, 103-127.
44. Rockwell, G. D.; Grindley, T. B., Effect of Solvation on the Rotation of Hydroxymethyl Groups in Carbohydrates. *J. Am. Chem. Soc.* **1998,** *120*, 10953-10963.
45. Spiwok, V.; Tvaroška, I., Metadynamics Modelling of the Solvent Effect on Primary Hydroxyl Rotamer Equilibria in Hexopyranosides. *Carbohydr. Res.* **2009,** *344*, 1575-1581.
46. Zuccarello, F.; Buemi, G., A Theoretical Study of D-Glucose, D-Galactose, and Parent Molecules: Solvent Effect on Conformational Stabilities and Rotational Motions of Exocyclic Groups. *Carbohydr. Res.* **1995,** *273*, 129-145.
47. Padron, J. I.; Morales, E. Q.; Vazquez, J. T., Alkyl Galactopyranosides: Rotational Population Dependence of the Hydroxymethyl Group on the Aglycon and Its Absolute Configuration and on the Anomeric Configuration. *J. Org. Chem.* **1998,** *63*, 8247-8258.
48. Padron, J. I.; Vazquez, J. T., Rotational Population Dependences of the Hydroxymethyl Group in Alkyl Glucopyranosides: Anomers Comparison. *Chirality* **1997,** *9*, 626-637.
49. Padron, J. I.; Vazquez, J. T., Stereochemical Study of the CD Spectral Differences between Anomers of Alkyl Glucopyranosides. *Tetrahedron-Asymmetry* **1998,** *9*, 613-627.
50. Liu, H. W.; Nakanishi, K., A Micromethod for Determining the Branching Points in Oligosaccharides Based on Circular Dichroism. *J. Am. Chem. Soc.* **1981,** *103*, 7005-7006.
51. Liu, H. W.; Nakanishi, K., Pyranose Benzoates: An Additivity Relation in the Amplitudes of Exciton-Split CD Curves. *J. Am. Chem. Soc.* **1982,** *104*, 1178-1185.
52. Morales, E. Q.; Padron, J. I.; Trujillo, M.; Vazquez, J. T., CD and $^{1}$H-NMR Study of the Rotational Population Dependence of the Hydroxymethyl Group in β-Glucopyranoside on the Aglycon and Its Absolute-Configuration. *J. Org. Chem.* **1995,** *60*, 2537-2548.
53. Damager, I.; Engelsen, S. B.; Blennow, A.; Moller, B. L.; Motawia, M. S., First Principles Insight into the α-Glucan Structures of Starch: Their Synthesis, Conformation, and Hydration. *Chem. Rev.* **2010,** *110*, 2049-2080.
54. Homans, S. W., Oligosaccharide Conformations: Application of NMR and Energy Calculations. *Prog. Nucl. Magn. Reson. Spectrosc.* **1990,** *22*, 55-81.
55. Kony, D. B.; Damm, W.; Stoll, S.; van Gunsteren, W. F.; Hünenberger, P. H., Explicit-Solvent Molecular Dynamics Simulations of the Polysaccharide Schizophyllan in Water. *Biophys. J.* **2007,** *93*, 442-455.
56. Yamada, H.; Harada, T.; Takahashi, T., Conformational Analysis of a Branched Sugar in Aqueous Solution Based on Molecular Mechanics and $^{1}$H-NMR Studies. *Tetrahedron Lett.* **1995,** *36*, 3185-3188.
57. Bernardi, A.; Colombo, A.; Sanchez-Medina, I., Conformational Analysis and Dynamics of Mannobiosides and Mannotriosides Using Monte Carlo/Stochastic Dynamics Simulations. *Carbohydr. Res.* **2004,** *339*, 967-973.
58. Best, R. B.; Jackson, G. E.; Naidoo, K. J., Molecular Dynamics and NMR Study of the α(1→4) and α(1→6) Glycosidic Linkages: Maltose and Isomaltose. *J. Phys. Chem. B* **2001,** *105*, 4742-4751.
59. Dowd, M. K.; French, A. D.; Reilly, P. J., Molecular Mechanics Modeling of α-(1→2)-Linked, α-(1→3)-Linked, and α-(1→6)-Linked Mannosyl Disaccharides with MM3(92). *J. Carbohydr. Chem.* **1995,** *14*, 589-600.

60. Hori, H.; Nishida, Y.; Ohrui, H.; Meguro, H.; Uzawa, J., Conformational Analyses of α and β (1→6) Mannodisaccharides by Deuterium Substitution Effect on Relaxation Rate and NOE. *Tetrahedron Lett.* **1988,** *29*, 4457-4460.
61. Jansson, P. E.; Kenne, L.; Kolare, I., NMR-Studies of Some (1→6)-Linked Disaccharide Methyl Glycosides. *Carbohydr. Res.* **1994,** *257*, 163-174.
62. Javaroni, F.; Ferreira, A. B. B.; da Silva, C. O., The (α-1,6) Glycosidic Bond of Isomaltose: A Tricky System for Theoretical Conformational Studies. *Carbohydr. Res.* **2009,** *344*, 1235-1247.
63. Mazumder, P.; Mukhopadhyay, C., Conformational Behavior of α-D-Mannopyranosyl-(1→6)-α,β-D-Mannose Complexed with Two Mannose-Binding Plant Lectins, *Allium sativam* Agglutinin I and Concanavalin A, Using NMR and Molecular Modeling Techniques. *Carbohydr. Res.* **2010,** *345*, 61-67.
64. Ohrui, H.; Nishida, Y.; Watanabe, M.; Hori, H.; Meguro, H., $^{1}$H-NMR Studies on (6*R*)- and (6*S*)-Deuterated (1→6)-Linked Disaccharides: Assignment of the Preferred Rotamers About C5–C6 Bond of (1→6)-Disaccharides in Solution. *Tetrahedron Lett.* **1985,** *26*, 3251-3254.
65. Cloran, F.; Carmichael, I.; Serianni, A. S., Density Functional Calculations on Disaccharide Mimics: Studies of Molecular Geometries and Trans-*O*-Glycosidic $^{3}J_{COCH}$ and $^{3}J_{COCC}$ Spin-Couplings. *J. Am. Chem. Soc.* **1999,** *121*, 9843-9851.
66. Mäler, L.; Widmalm, G.; Kowalewski, J., Motional Properties of a Pentasaccharide Containing a 2,6-Branched Mannose Residue as Studied by $^{13}$C Nuclear Spin Relaxation. *J. Biomol. NMR* **1996,** *7*, 1-7.
67. Salisburg, A. M.; Deline, A. L.; Lexa, K. W.; Shields, G. C.; Kirschner, K. N., Ramachandran-Type Plots for Glycosidic Linkages: Examples from Molecular Dynamic Simulations Using the GLYCAM06 Force Field. *J. Comput. Chem.* **2009,** *30*, 910-921.
68. Kirschner, K. N.; Yongye, A. B.; Tschampel, S. M.; González-Outeiriño, J.; Daniels, C. R.; Foley, B. L.; Woods, R. J., GLYCAM06: A Generalizable Biomolecular Force Field. Carbohydrates. *J. Comput. Chem.* **2008,** *29*, 622-655.
69. Kony, D.; Damm, W.; Stoll, S.; van Gunsteren, W. F., An Improved OPLS-AA Force Field for Carbohydrates. *J. Comput. Chem.* **2002,** *23*, 1416-1429.
70. Kony, D.; Damm, W.; Stoll, S.; Hünenberger, P. H., Explicit-Solvent Molecular Dynamics Simulations of the β(1→3)- and β(1→6)-Linked Disaccharides β-Laminarabiose and β-Gentiobiose in Water. *J. Phys. Chem. B* **2004,** *108*, 5815-5826.
71. Eklund, R.; Widmalm, G., Molecular Dynamics Simulations of an Oligosaccharide Using a Force Field Modified for Carbohydrates. *Carbohydr. Res.* **2003,** *338*, 393-398.
72. Lins, R. D.; Hünenberger, P. H., A New GROMOS Force Field for Hexopyranose-Based Carbohydrates. *J. Comput. Chem.* **2005,** *26*, 1400-1412.
73. Pereira, C. S.; Kony, D.; Baron, R.; Müller, M.; van Gunsteren, W. F.; Hünenberger, P. H., Conformational and Dynamical Properties of Disaccharides in Water: A Molecular Dynamics Study. *Biophys. J.* **2006,** *90*, 4337-4344.
74. Perić-Hassler, L.; Hansen, H. S.; Baron, R.; Hünenberger, P. H., Conformational Properties of Glucose-Based Disaccharides Investigated Using Molecular Dynamics Simulations with Local Elevation Umbrella Sampling. *Carbohydr. Res.* **2010,** *345*, 1781-1801.
75. MacKerell, A. D., Jr., Empirical Force Fields for Biological Macromolecules: Overview and Issues. *J. Comput. Chem.* **2004,** *25*, 1584-1604.

76. Pendrill, R.; Säwén, E.; Widmalm, G., Conformation and Dynamics at a Flexible Glycosidic Linkage Revealed by NMR Spectroscopy and Molecular Dynamics Simulations: Analysis of β-L-Fucp-(1→6)-α-D-Glcp-OMe in Water Solution. *J. Phys. Chem. B* **2013,** *117*, 14709-14722.
77. Kotsyubynskyy, D.; Zerbetto, M.; Soltesova, M.; Engström, O.; Pendrill, R.; Kowalewski, J.; Widmalm, G.; Polimeno, A., Stochastic Modeling of Flexible Biomolecules Applied to NMR Relaxation. 2. Interpretation of Complex Dynamics in Linear Oligosaccharides. *J. Phys. Chem. B* **2012,** *116*, 14541-14555.
78. Guvench, O.; Hatcher, E.; Venable, R. M.; Pastor, R. W.; MacKerell, A. D., Jr., CHARMM Additive All-Atom Force Field for Glycosidic Linkages between Hexopyranoses. *J. Chem. Theory Comput.* **2009,** *5*, 2353-2370.
79. Guvench, O.; Mallajosyula, S. S.; Raman, E. P.; Hatcher, E.; Vanommeslaeghe, K.; Foster, T. J.; Jamison, F. W., II; MacKerell, A. D., Jr., CHARMM Additive All-Atom Force Field for Carbohydrate Derivatives and Its Utility in Polysaccharide and Carbohydrate-Protein Modeling. *J. Chem. Theory Comput.* **2011,** *7*, 3162-3180.
80. Hatcher, E. R.; Guvench, O.; MacKerell, A. D., Jr., CHARMM Additive All-Atom Force Field for Acyclic Polyalcohols, Acyclic Carbohydrates, and Inositol. *J. Chem. Theory Comput.* **2009,** *5*, 1315-1327.
81. Mallajosyula, S. S.; Guvench, O.; Hatcher, E.; MacKerell, A. D., Jr., CHARMM Additive All-Atom Force Field for Phosphate and Sulfate Linked to Carbohydrates. *J. Chem. Theory Comput.* **2012,** *8*, 759-776.
82. Raman, E. P.; Guvench, O.; MacKerell, A. D., Jr., CHARMM Additive All-Atom Force Field for Glycosidic Linkages in Carbohydrates Involving Furanoses. *J. Phys. Chem. B* **2010,** *114*, 12981-12994.
83. Kamath, G.; Guvench, O.; MacKerell, A. D., Jr., CHARMM Additive All-Atom Force Field for Acyclic Carbohydrates and Inositol. *J. Chem. Theory Comput.* **2008,** *4*, 765-778.
84. Lycknert, K.; Edblad, M.; Imberty, A.; Widmalm, G., NMR and Molecular Modeling Studies of the Interaction between Wheat Germ Agglutinin and the β-D-Glc*p*NAc-(1→6)-α-D-Man*p* Epitope Present in Glycoproteins of Tumor Cells. *Biochemistry* **2004,** *43*, 9647-9654.
85. Rönnols, J.; Pendrill, R.; Fontana, C.; Hamark, C.; d'Ortoli, T. A.; Engström, O.; Ståhle, J.; Zaccheus, M. V.; Säwén, E.; Hahn, L. E.; Iqbal, S.; Widmalm, G., Complete $^{1}$H and $^{13}$C NMR Chemical Shift Assignments of Mono- to Tetrasaccharides as Basis for NMR Chemical Shift Predictions of Oligosaccharides Using the Computer Program CASPER. *Carbohydr. Res.* **2013,** *380*, 156-166.
86. Roslund, M. U.; Säwén, E.; Landström, J.; Rönnols, J.; Jonsson, K. H. M.; Lundborg, M.; Svensson, M. V.; Widmalm, G., Complete $^{1}$H and $^{13}$C NMR Chemical Shift Assignments of Mono-, Di-, and Trisaccharides as Basis for NMR Chemical Shift Predictions of Polysaccharides Using the Computer Program CASPER. *Carbohydr. Res.* **2011,** *346*, 1311-1319.
87. Zerbetto, M.; Polimeno, A.; Kotsyubynskyy, D.; Ghalebani, L.; Kowalewski, J.; Meirovitch, E.; Olsson, U.; Widmalm, G., An Integrated Approach to NMR Spin Relaxation in Flexible Biomolecules: Application to β-D-Glucopyranosyl-(1→6)-α-D-Mannopyranosyl-OMe. *J. Chem. Phys.* **2009,** *131*, 234501-234510.

88. Laatikainen, R.; Niemitz, M.; Weber, U.; Sundelin, J.; Hassinen, T.; Vepsäläinen, J., General Strategies for Total-Lineshape-Type Spectral Analysis of NMR Spectra Using Integral-Transform Iterator. *J. Magn. Reson., Ser A* **1996,** *120*, 1-10.
89. Meissner, A.; Sørensen, O. W., Measurement of *J*(H,H) and Long-Range *J*(X,H) Coupling Constants in Small Molecules. Broadband XLOC and J-HMBC. *Magn. Reson. Chem.* **2001,** *39*, 49-52.
90. Koźmiński, W.; Nanz, D., HECADE: HMQC- and HSQC-Based 2D NMR Experiments for Accurate and Sensitive Determination of Heteronuclear Coupling Constants from E.COSY-Type Cross Peaks. *J. Magn. Reson.* **1997,** *124*, 383-392.
91. Stott, K.; Stonehouse, J.; Keeler, J.; Hwang, T-L.; Shaka, A. J., Excitation Sculpting in High-Resolution Nuclear Magnetic Resonance Spectroscopy: Application to Selective NOE Experiments. *J. Am. Chem. Soc.* **1995,** *117*, 4199-4200.
92. Thrippleton, M. J.; Keeler, J., Elimination of Zero-Quantum Interference in Two-Dimensional NMR Spectra. *Angew. Chem., Int. Ed.* **2003,** *42*, 3938-3941.
93. Kupče, Ē.; Boyd, J.; Campbell, I. D., Short Selective Pulses for Biochemical Applications. *J. Magn. Reson., Ser B* **1995,** *106*, 300-303.
94. Hu, H.; Krishnamurthy, K., Revisiting the Initial Rate Approximation in Kinetic NOE Measurements. *J. Magn. Reson.* **2006,** *182*, 173-177.
95. Jonsson, K. H. M.; Pendrill, R.; Widmalm, G., NMR Analysis of Conformationally Dependent $^{n}J_{C,H}$ and $^{n}J_{C,C}$ in the Trisaccharide α-L-Rhap-(1→2)[α-L-Rha*p*-(1→3)]-α-L-Rha*p*-OMe and a Site-Specifically Labeled Isotopologue Thereof. *Magn. Reson. Chem.* **2011,** *49*, 117-124.
96. Frisch, M. J.; Trucks, G. W.; Schlegel, H. B.; Scuseria, G. E.; Robb, M. A.; Cheeseman, J. R.; Montgomery, J. J. A.; Vreven, T.; Kudin, K. N.; Burant, J. C.; et al., *Gaussian 03*, Gaussian, Inc., Wallingford CT: 2003.
97. Brooks, B. R.; Brooks, C. L., III; MacKerell, A. D., Jr.; Nilsson, L.; Petrella, R. J.; Roux, B.; Won, Y.; Archontis, G.; Bartels, C.; Boresch, S.; et al., CHARMM: The Biomolecular Simulation Program. *J. Comput. Chem.* **2009,** *30*, 1545-1614.
98. Jorgensen, W. L.; Chandrasekhar, J.; Madura, J. D.; Impey, R. W.; Klein, M. L., Comparison of Simple Potential Functions for Simulating Liquid Water *J. Chem. Phys.* **1983,** *79*, 926-935.
99. *Computational Biochemistry and Biophysics*; Becker, O. M.; MacKerell, A. D., Jr., Roux, B.; Watanabe, M., Eds.; Marcel-Dekker Inc.: New York, 2001.
100. Brooks, C. L., III.; Karplus, M.; Pettitt, B. M., *Proteins: A Theoretical Perspective of Dynamics, Structure and Thermodynamics*. John Wiley & Sons: New York, 1988.
101. Darden, T.; York, D.; Pedersen, L., Particle Mesh Ewald: An $N\cdot\log(N)$ Method for Ewald Sums in Large Systems *J. Chem. Phys.* **1993,** *98*, 10089-10092.
102. Steinbach, P. J.; Brooks, B. R., New Sperical-Cutoff Methods for Long-Range Forces in Macromolecular Simulation. *J. Comput. Chem.* **1994,** *15*, 667-683.
103. Ryckaert, J-P.; Ciccotti, G.; Berendsen, H. J. C., Numerical Integration of the Cartesian Equations of Motion of a System with Constraints: Molecular Dynamics of *n*-Alkanes. *J. Comput. Phys.* **1977,** *23*, 327-341.
104. Beglov, D.; Roux, B., An Integral Equation to Describe the Solvation of Polar Molecules in Liquid Water. *J. Phys. Chem. B* **1997,** *101*, 7821-7826.

105. Woodcock, H. L., III; Hodoscek, M.; Gilbert, A. T. B.; Gill, P. M. W.; Schaefer, H. F., III; Brooks, B. R., Interfacing Q-Chem and CHARMM to Perform QM/MM Reaction Path Calculations. *J. Comput. Chem.* **2007,** *28*, 1485-1502.
106. Faraldo-Gómez, J. D.; Roux, B., Characterization of Conformational Equilibria through Hamiltonian and Temperature Replica-Exchange Simulations: Assessing Entropic and Environmental Effects. *J. Comput. Chem.* **2007,** *28*, 1634-1647.
107. Wolf, M. G.; de Leeuw, S. W., Fast in Silico Protein Folding by Introduction of Alternating Hydrogen Bond Potentials. *Biophys. J.* **2008,** *94*, 3742-3747.
108. Jiang, W.; Roux, B., Free Energy Perturbation Hamiltonian Replica-Exchange Molecular Dynamics (FEP/H-REMD) for Absolute Ligand Binding Free Energy Calculations. *J. Chem. Theory Comput.* **2010,** *6*, 2559-2565.
109. Mallajosyula, S. S.; MacKerell, A. D., Jr., Influence of Solvent and Intramolecular Hydrogen Bonding on the Conformational Properties of O-Linked Glycopeptides. *J. Phys. Chem. B* **2011,** *115*, 11215-11229.
110. Kannan, S.; Zacharias, M., Folding of Trp-Cage Mini Protein Using Temperature and Biasing Potential Replica-Exchange Molecular Dynamics Simulations. *Intl. J. Mol. Sci.* **2009,** *10*, 1121-1137.
111. Vreede, J.; Wolf, M. G.; de Leeuw, S. W.; Bolhuis, P. G., Reordering Hydrogen Bonds Using Hamiltonian Replica Exchange Enhances Sampling of Conformational Changes in Biomolecular Systems. *J. Phys. Chem. B* **2009,** *113*, 6484-6494.
112. Buck, M.; Bouguet-Bonnet, S.; Pastor, R. W.; MacKerell, A. D., Jr., Importance of the CMAP Correction to the CHARMM22 Protein Force Field: Dynamics of Hen Lysozyme. *Biophys. J.* **2006,** *90*, L36-L38.
113. MacKerell, A. D., Jr.; Feig, M.; Brooks, C. L., Extending the Treatment of Backbone Energetics in Protein Force Fields: Limitations of Gas-Phase Quantum Mechanics in Reproducing Protein Conformational Distributions in Molecular Dynamics Simulations. *J. Comput. Chem.* **2004,** *25*, 1400-1415.
114. Haasnoot, C. A. G.; de Leeuw, F. A. A. M.; Altona, C., The Relationship between Proton-Proton NMR Coupling Constants and Substituent Electronegativities—I: An Empirical Generalization of the Karplus Equation. *Tetrahedron* **1980,** *36*, 2783-2792.
115. Imai, K.; Ōsawa, E., An Empirical Extension of the Karplus Equation. *Magn. Reson. Chem.* **1990,** *28*, 668-674.
116. Stenutz, R.; Carmichael, I.; Widmalm, G.; Serianni, A. S., Hydroxymethyl Group Conformation in Saccharides: Structural Dependencies of $^{2}J_{HH}$, $^{3}J_{HH}$, and $^{1}J_{CH}$ Spin-Spin Coupling Constants. *J. Org. Chem.* **2002,** *67*, 949-958.
117. Thibaudeau, C.; Stenutz, R.; Hertz, B.; Klepach, T.; Zhao, S.; Wu, Q. Q.; Carmichael, I.; Serianni, A. S., Correlated C-C and C-O Bond Conformations in Saccharide Hydroxymethyl Groups: Parametrization and Application of Redundant $^{1}$H-$^{1}$H, $^{13}$C-$^{1}$H, and $^{13}$C-$^{13}$C NMR *J*-Couplings. *J. Am. Chem. Soc.* **2004,** *126*, 15668-15685.
118. Säwén, E.; Massad, T.; Landersjö, C.; Damberg, P.; Widmalm, G., Population Distribution of Flexible Molecules from Maximum Entropy Analysis Using Different Priors as Background Information: Application to the ϕ, ψ-Conformational Space of the α-(1→2)-Linked Mannose Disaccharide Present in *N*- and *O*-Linked Glycoproteins. *Org. Biomol. Chem.* **2010,** *8*, 3684-3695.
119. Roen, A.; Mayato, C.; Padron, J. I.; Vazquez, J. T., Conformational Domino Effect in Saccharides. 2. Anomeric Configuration Control. *J. Org. Chem.* **2008,** *73*, 7266-7279.

120. Roen, A.; Padron, J. I.; Mayato, C.; Vazquez, J. T., Conformational Domino Effect in Saccharides: A Prediction from Alkyl β-(1→6)-Diglucopyranosides. *J. Org. Chem.* **2008,** *73*, 3351-3363.
121. Roen, A.; Padron, J. I.; Vazquez, J. T., Hydroxymethyl Rotamer Populations in Disaccharides. *J. Org. Chem.* **2003,** *68*, 4615-4630.
122. Landersjö, C.; Stenutz, R.; Widmalm, G., Conformational Flexibility of Carbohydrates: A Folded Conformer at the ϕ Dihedral Angle of a Glycosidic Linkage. *J. Am. Chem. Soc.* **1997,** *119*, 8695-8698.
123. Nishida, Y.; Hori, H.; Ohrui, H.; Meguro, H.; Uzawa, J.; Reimer, D.; Sinnwell, V.; Paulsen, H., Conformational Analyses of O4,O6-Branching Tri-D-Glucopyranosides; Influence of O4 Linked Residues on Solution Conformations About C5-C6 Bonds at (1→6)-Linkages. *Tetrahedron Lett.* **1988,** *29*, 4461-4464.
124. Poppe, L., Modeling Carbohydrate Conformations from NMR Data - Maximum Entropy Rotameric Distribution About the C5-C6 Bond in Gentiobiose. *J. Am. Chem. Soc.* **1993,** *115*, 8421-8426.
125. Tachibana, Y.; Fletcher, G. L.; Fujitani, N.; Tsuda, S.; Monde, K.; Nishimura, S. I., Antifreeze Glycoproteins: Elucidation of the Structural Motifs That Are Essential for Antifreeze Activity. *Angew. Chem. Int. Ed.* **2004,** *43*, 856-862.
126. Harding, M. M.; Anderberg, P. I.; Haymet, A. D. J., 'Antifreeze' Glycoproteins from Polar Fish. *Eur. J. Biochem.* **2003,** *270*, 1381-1392.
127. Eriksson, L.; Widmalm, G., Amygdalin Trihydrate. *Acta Crystallogr., Sect. E* **2005,** *61*, O860-O862.
128. Berman, E., Structural and Conformational Analysis of Sialyloligosaccharides Using Carbon-13 Nuclear Magnetic Resonance Spectroscopy. *Biochemistry* **1984,** *23*, 3754-3759.
129. Sabesan, S.; Paulson, J. C., Combined Chemical and Enzymatic Synthesis of Sialyloligosaccharides and Characterization by 500-MHz and $^{1}H$ and $^{13}C$ NMR Spectroscopy. *J. Am. Chem. Soc.* **1986,** *108*, 2068-2080.
130. Poppe, L.; Stuike-Prill, R.; Meyer, B.; van Halbeek, H., The Solution Conformation of Sialyl-α(2→6)-Lactose Studied by Modern NMR Techniques and Monte-Carlo Simulations. *J. Biomol. NMR* **1992,** *2*, 109-136.
131. Sabesan, S.; Bock, K.; Paulson, J. C., Conformational Analysis of Sialyloligosaccharides. *Carbohydr. Res.* **1991,** *218*, 27-54.
132. Ohrui, H.; Nishida, Y.; Itoh, H.; Meguro, H., Preferred Conformation About the C5-C6 Bond of *N*-Acetylneurminyl(2→6)-D-Galacto- and -D-Glucopyranosides in Solution. *J. Org. Chem.* **1991,** *56*, 1726-1731.
133. Lee, K.; Gu, S.; Jin, L.; Le, T. T.; Cheng, L. W.; Strotmeier, J.; Kruel, A. M.; Yao, G.; Perry, K.; Rummel, A.; Jin, R., Structure of a Bimodular Botulinum Neurotoxin Complex Provides Insights into Its Oral Toxicity. *PLoS Pathog.* **2013,** *9*, e1003690.

**Table of Contents Image**